

Regular Article*Highlighted Paper selected by Editor-in-Chief***Discovery of a Novel Series of Pyrazolo[1,5-*a*]pyrimidine-Based Phosphodiesterase 2A Inhibitors Structurally Different from *N*-((1*S*)-1-(3-Fluoro-4-(trifluoromethoxy)phenyl)-2-methoxyethyl)-7-methoxy-2-oxo-2,3-dihydropyrido[2,3-*b*]pyrazine-4(1*H*)-carboxamide (TAK-915), for the Treatment of Cognitive Disorders**

Satoshi Mikami,^{*a} Masanori Kawasaki,^a Shuhei Ikeda,^a Nobuyuki Negoro,^a Shinji Nakamura,^a Izumi Nomura,^a Tomoko Ashizawa,^a Hironori Kokubo,^a Isaac Dylan Hoffman,^b Hua Zou,^b Hideyuki Oki,^a Noriko Uchiyama,^a Yuuto Hiura,^{a,†} Maki Miyamoto,^a Yuuki Itou,^a Masato Nakashima,^a Hiroki Iwashita,^a and Takahiko Taniguchi^a

^aPharmaceutical Research Division, Takeda Pharmaceutical Company, Limited; 2–26–1 Muraoka-Higashi, Fujisawa, Kanagawa 251–8555, Japan; and ^bTakeda California, Inc.; 10410 Science Center Drive, San Diego, California 92121, United States.

Received July 12, 2017; accepted August 14, 2017

It has been hypothesized that selective inhibition of phosphodiesterase (PDE) 2A could potentially be a novel approach to treat cognitive impairment in neuropsychiatric and neurodegenerative disorders through augmentation of cyclic nucleotide signaling pathways in brain regions associated with learning and memory. Following our earlier work, this article describes a drug design strategy for a new series of lead compounds structurally distinct from our clinical candidate 2 (TAK-915), and subsequent medicinal chemistry efforts to optimize potency, selectivity over other PDE families, and other preclinical properties including *in vitro* phototoxicity and *in vivo* rat plasma clearance. These efforts resulted in the discovery of *N*-((1*S*)-2-hydroxy-2-methyl-1-(4-(trifluoromethoxy)phenyl)propyl)-6-methyl-5-(3-methyl-1*H*-1,2,4-triazol-1-yl)pyrazolo[1,5-*a*]pyrimidine-3-carboxamide (20), which robustly increased 3',5'-cyclic guanosine monophosphate (cGMP) levels in the rat brain following an oral dose, and moreover, attenuated MK-801-induced episodic memory deficits in a passive avoidance task in rats. These data provide further support to the potential therapeutic utility of PDE2A inhibitors in enhancing cognitive performance.

Key words phosphodiesterase 2A; schizophrenia; pyrazolo[1,5-*a*]pyrimidine; structure-based drug design; phototoxicity; intramolecular hydrogen bond

Schizophrenia is a chronic, severe, and disabling mental disorder affecting approximately 1% of the general population worldwide,^{1–4)} resulting in profound disruption in emotion and cognition, which has a major impact on patients' and caregivers' lives. The symptoms can typically be divided into three domains: positive (delusions and hallucinations), negative (lack of motivation and social withdrawal), and cognitive (memory, attention, and executive function) symptoms. The most recent medications commonly prescribed for schizophrenia include a new generation of antipsychotics called atypical or second-generation antipsychotics (SGAs), which function *via* inhibition of dopamine D2 and serotonin 5-HT_{2A} receptors.⁵⁾ It has been reported that these agents are reasonably effective at treating the positive symptoms of schizophrenia, but show little or no efficacy against negative and cognitive symptoms of the disease.⁶⁾ Furthermore, although generally more effective and better tolerated than typical or first-generation antipsychotics (FGAs), atypical antipsychotics also cause a variety of drug-related side effects such as sedation, weight gain, an increased risk of type II diabetes and high cholesterol, extrapyramidal symptoms, hypotension, and prolactin elevation.^{7–9)} Thus, there is a clear and high unmet medical need for a

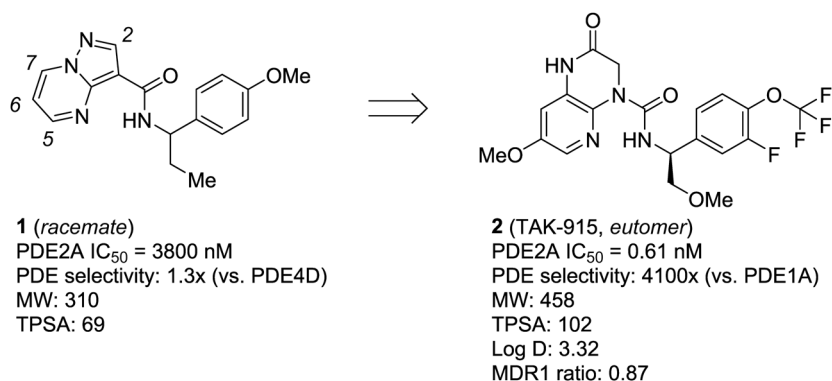
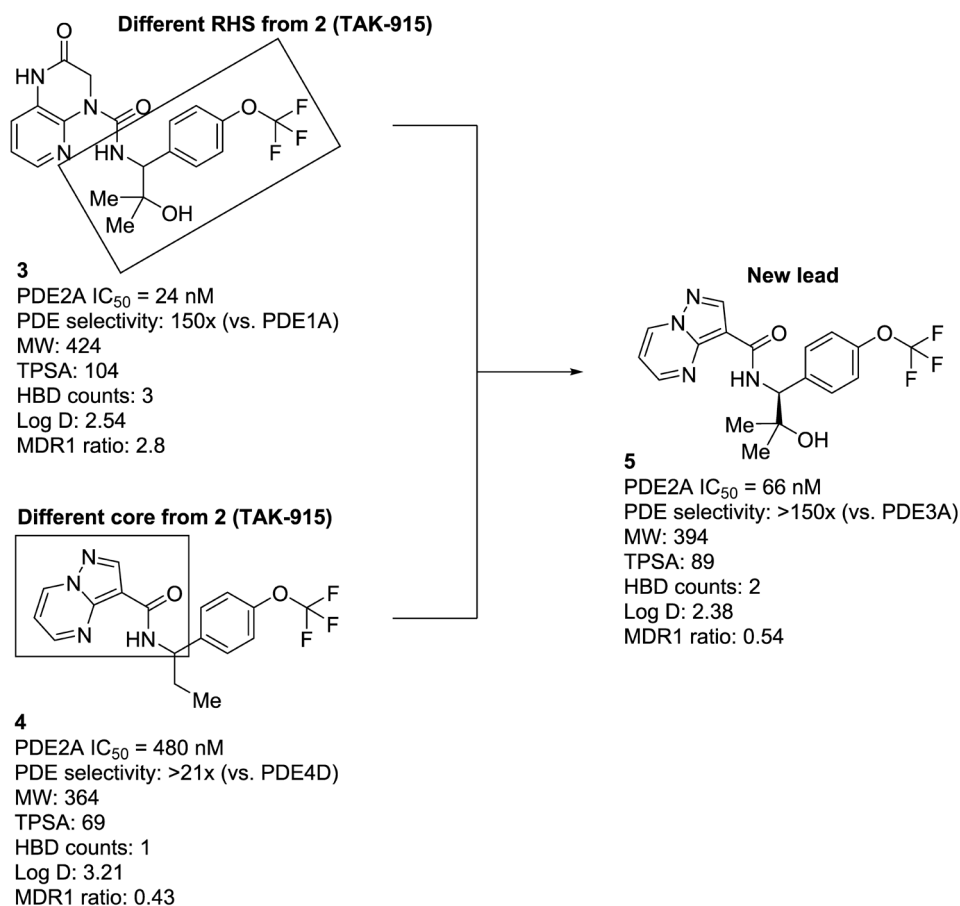
novel antipsychotic with improved efficacy and superior safety profile for the treatment of schizophrenia, especially against negative and cognitive symptoms of the disease.

Owing to a growing body of preclinical research, phosphodiesterase (PDE) 2A has been recently receiving significant attention for its therapeutic potential to treat central nervous system (CNS) disorders, including schizophrenia and Alzheimer's disease.^{10–41)} PDE2A is one of the 11 known PDE families and is highly expressed in brain regions such as the striatum, hippocampus, and frontal cortex, which are closely linked to emotion, learning, and memory.^{13–18)} In addition, PDE2A has been shown to hydrolyze the intracellular second messengers, cAMP and 3',5'-cyclic guanosine monophosphate (cGMP),¹⁹⁾ molecules that play important roles in regulating cyclic nucleotide signaling implicated in neuronal plasticity and memory.^{20–24)} In light of these features, it is hypothesized that inhibition of PDE2A could exert procognitive activity through augmentation of cyclic nucleotide signaling in the aforementioned brain areas, thus leading to the treatment of cognitive dysfunction in a range of neuropsychiatric and neurodegenerative disorders.

On the basis of this biological hypothesis, we initiated a drug discovery program to develop PDE2A inhibitors. A series of recent publications from our research group described medicinal chemistry efforts^{42,43)} leading to the identification

[†]Present address: University of Fukui School of Medical Sciences; 23–3 Matsuokashimoaizuki, Eiheiji-cho, Yoshida, Fukui 910–1193, Japan.

* To whom correspondence should be addressed. e-mail: satoshi.mikami@takeda.com

Fig. 1. Transition from High-Throughput Screening Hit **1** to Clinical Candidate **2** (TAK-915)Fig. 2. Origin of a Novel PDE2A Lead Compound **5**

of clinical candidate **2** (TAK-915^{35,43}) originating from high-throughput screening hit **1** (Fig. 1). Over the course of the discovery of **2**, we identified another novel right-hand side (RHS) benzylamine moiety structurally distinct from **2**, as exemplified by compound **3** (Fig. 2). Although compound **3** exhibited a good balance of potency and PDE selectivity, it was found to be a P-glycoprotein (P-gp) substrate as evidenced by high multidrug resistance protein 1 (MDR1) efflux ratio, resulting in lower brain exposure. On the other hand, the previously described pyrazolo[1,5-*a*]pyrimidine series, as represented by compound **4**, demonstrated favorable MDR1 efflux ratios, but had suboptimal PDE2A inhibitory activity due to an unoptimized core and RHS benzylamine moieties.⁴² With these attributes of the two compound classes in mind, we combined

structural features from both chemotypes to deliver a new class of lead with no MDR1 liability. Despite the fact that compounds **2** and **3** possess a nearly identical topological polar surface area (TPSA), the former has a superior MDR1 efflux ratio, indicating that the hydrogen bond donor (HBD) count (two HBDs in **2** vs. three HBDs in **3**) may play a crucial role in defining each compound as a P-gp substrate.^{44,45} We therefore reasoned that replacing the 3,4-dihydropyrido[2,3-*b*]pyrazin-2(*1H*)-one core in **3** with the pyrazolo[1,5-*a*]pyrimidine core derived from **4** would serve to improve brain penetration by reducing the overall HBD count. Indeed, hybrid compound **5** showed reasonable inhibition of PDE2A with an IC₅₀ of 66 nM and no indication of being a P-gp substrate. These promising attributes of **5** as a lead compound encour-

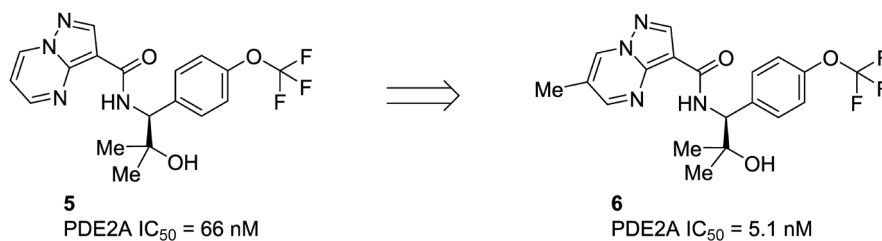
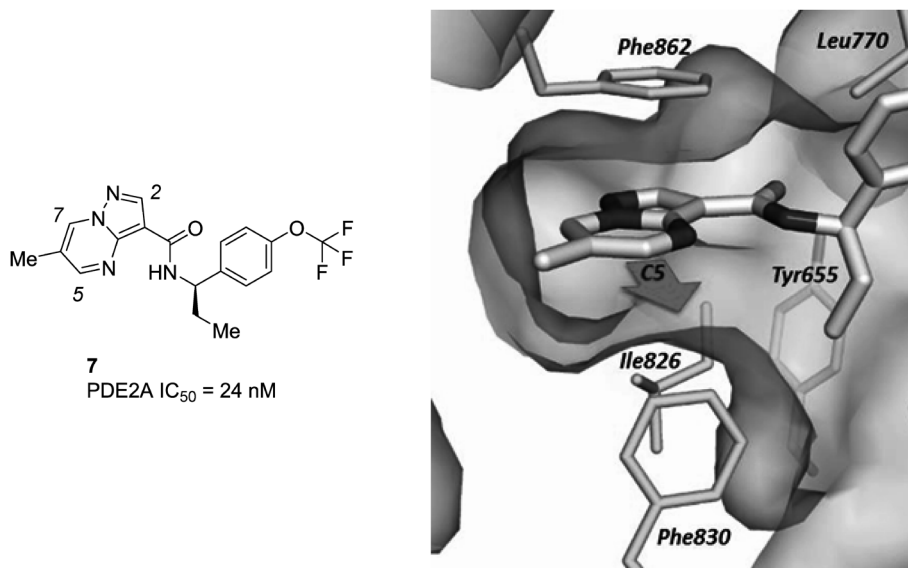


Fig. 3. Effect of a 6-Methyl Substitution on PDE2A Inhibitory Activity

Fig. 4. X-Ray Crystal Structure of **7** Bound in the PDE2A Catalytic Site (PDB 5XKM)

aged us to focus on further optimization, aiming mainly to improve inhibitory activity.

Our previous structure–activity relationship (SAR) study of methyl substitutions on the pyrazolo[1,5-*a*]pyrimidine core of **1** demonstrated that the 6-methyl substitution provided an approximately 10-fold increase in the PDE2A inhibitory activity (see Fig. 1 for numbering of the substitution positions). The 5-methyl substitution was well tolerated, while the introduction of the methyl group into the 2- or 7-position was detrimental for potency.⁴²⁾ In good agreement with the previous SAR, introduction of the methyl group at the 6-position of compound **5** to give compound **6** (Fig. 3) resulted in a 13-fold boost in potency. An X-ray crystal structure of compound **7** bound to PDE2A revealed an unoccupied and relatively large hydrophobic space around the 5-position of the core (Fig. 4); this finding supported the tolerance for the 5-methyl substitution. These findings provided an avenue for further elaboration at the 5-position (R^1 of the structure in Fig. 5) that might lead to potency enhancement. Overall, with the aim of further increasing the inhibitory activity to the levels of our leading clinical candidate **2** (IC₅₀=0.61 nM), our medicinal chemistry effort was focused on variations of substituents at the 5 and 6-positions of the pyrazolo[1,5-*a*]pyrimidine core. Taking into account synthetic tractability, we initially chose to prepare 5-substituted pyrazolo[1,5-*a*]pyrimidine analogs with no methyl group at the 6-position (R^2 =H of the structure in Fig. 5).

Herein, we describe the SAR of 5- and/or 6-substituted pyrazolo[1,5-*a*]pyrimidine derivatives, culminating in the discovery of highly potent, selective, orally bioavailable,

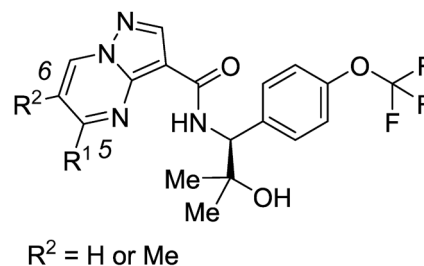
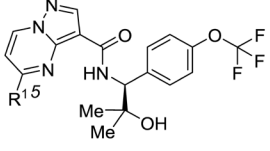


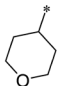
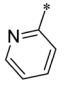
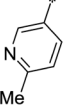
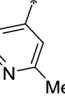
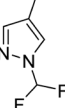
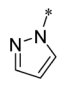
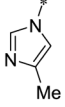
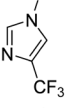
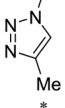
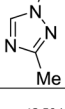
Fig. 5. Drug Design Strategies to Further Increase Potency

and brain-penetrating PDE2A inhibitors, as represented by *N*-((1*S*)-2-hydroxy-2-methyl-1-(4-(trifluoromethoxy)phenyl)propyl)-6-methyl-5-(3-methyl-1*H*-1,2,4-triazol-1-yl)pyrazolo[1,5-*a*]pyrimidine-3-carboxamide (**20**). This new series successfully overcame *in vitro* phototoxicity issues identified by the introduction of substituents at the 5-position of the core. In addition, we report an X-ray crystal structure of **20** bound in the PDE2A active site to better understand the origin of high potency and PDE selectivity, as well as *in vivo* data linking target engagement and pharmacodynamic (PD) effects to relevant *in vivo* efficacy in a preclinical model of cognitive impairment.

Results and Discussion

Table 1 summarizes the effects of carbon-linked substitutions at the 5-position of the pyrazolo[1,5-*a*]pyrimidine core. The corresponding data for **5** are also included in the table for

Table 1. Profiles of Pyrazolo[1,5-*a*]pyrimidine Derivatives with Substitutions at the 5-Position


compd	R ¹	PDE2A IC ₅₀ (nM) ^a	PDE selectivity ^b	MDR1 ^c	rat in vivo CL (mL/h/kg) ^d	phototox (%) ^e	LogD ^f
5	H	66 (41–110)	>150-fold	0.54	632	–0.1	2.38
8	<i>i</i> -Pr	34 (24–49)	190-fold	0.48	NT	–9.2	3.30
9		10 (5.2–19)	NT	3.6	4142	–6.6	2.82
10		1.2 (0.80–1.8)	2700-fold	0.52	381	102.1	3.48
11		0.98 (0.61–1.6)	3800-fold	0.80	2361	78.9	3.38
12		0.77 (0.44–1.4)	1400-fold	0.80	4350	108.7	3.22
13		1.7 (1.2–2.5)	1300-fold	1.2	558	102.1	3.14
14		5.4 (3.4–8.7)	630-fold	0.54	353	11.0	3.29
15		1.2 (0.94–1.6)	1900-fold	5.2	NT	–1.0	3.08
16		7.1 (4.6–11)	230-fold	2.1	637	11.8	3.42
17		5.4 (3.5–8.3)	690-fold	0.73	476	7.5 ^g	3.12
18		11 (8.8–14)	610-fold	0.90	779	3.8	3.15

^a IC₅₀ values (95% confidence intervals given in parentheses) were calculated from percent inhibition data (duplicate, *n* = 1). All values are rounded off to two significant digits. ^b Minimum selectivity (rounded off to two significant digits) over other PDEs. ^c MDR1 efflux ratios in P-glycoprotein (P-gp)-overexpressing cells. ^d Plasma clearance calculated following 0.1 mg/kg, i.v. cassette dosing in rats (non-fasted). ^e Values (%) represent the difference between viability of cells exposed to 50 μM of the test compound in the absence of UV irradiation and that in the presence of UV irradiation, where cell viability was measured by intracellular ATP content (%) at 50 μM relative to vehicle control. A larger value is interpreted as a higher risk of phototoxicity. ^f LogD values at pH 7.4. ^g Precipitates observed.

comparison. Introducing an isopropyl group at the 5-position (**8**) had little impact on potency relative to the non-substituted analog **5**, while the introduction of a bigger and less lipophilic tetrahydro-2*H*-pyran group (**9**) tended to show moderately

improved activity. However, compound **9** displayed an unfavorable MDR1 efflux ratio and high *in vivo* clearance, likely being driven by increased polarity due to the tetrahydro-2*H*-pyran group, and increased number of methylene moieties

Table 2. Profiles of Di-substituted Pyrazolo[1,5-*a*]pyrimidine Derivatives

compd	R ¹	PDE2A IC ₅₀ (nM) ^a	PDE selectivity ^b	MDR1 ^c	rat in vivo CL (mL/h/kg) ^d	phototox (%) ^e	LogD ^f
6	H	5.1 (4.3–6.1)	1600-fold	0.53	2743	4.2	2.66
19		0.31 (0.27–0.35)	5800-fold	1.2	940	13.0 ^g	3.24
20		0.51 (0.46–0.58)	5300-fold	1.0	1169	3.7	3.42

a) IC₅₀ values (95% confidence intervals given in parentheses) were calculated from percent inhibition data (duplicate, *n*=1). All values are rounded off to two significant digits. b) Minimum selectivity (rounded off to two significant digits) over other PDEs. c) MDR1 efflux ratios in P-glycoprotein (P-gp)-overexpressing cells. d) Plasma clearance calculated following 0.1 mg/kg, i.v. cassette dosing in rats (non-fasted). e) Values (%) represent the difference between viability of cells exposed to 50 μM of the test compound in the absence of UV irradiation and that in the presence of UV irradiation, where cell viability was measured by intracellular ATP content (%) at 50 μM relative to vehicle control. A larger value is interpreted as a higher risk of phototoxicity. f) LogD values at pH 7.4. g) Precipitates observed.

Table 3. Inhibitory Activities of **19** and **20** against Human PDEs^{a)}

Compd.	PDE1A	PDE2A	PDE3A	PDE4D2	PDE5A1	PDE6AB	PDE7B	PDE8A1	PDE9A2	PDE10A2	PDE11A4
19	3300	0.31	>10000	3300	8800	1800	>10000	>10000	>10000	1700	3000
20	2700	0.51	>10000	9400	9100	8000	>10000	>10000	>10000	3100	6100

a) IC₅₀ values (nM) were calculated from percent inhibition data (duplicate, *n*=1). All values are rounded off to two significant digits.

susceptible to oxidative metabolism, respectively. To address such liabilities of the aliphatic heterocycle, we next sought to add heteroaryl groups. The 2-pyridyl substitution in compound **10** provided not only dramatically improved potency and excellent selectivity over other PDEs, but also a favorable MDR1 efflux ratio and significantly reduced *in vivo* clearance. In addition, 3- and 4-pyridine derivatives **11** and **12**, respectively, retained desirable attributes of the 2-pyridine derivative **10**, including inhibitory activity, PDE selectivity and MDR1 efflux ratio; however, they showed increased *in vivo* clearance probably due to oxidation of the methyl groups adjacent to the pyridine nitrogen atoms and/or *N*-oxidation of the pyridines. To overcome the potential metabolic liability of the methylpyridine derivatives, the difluoromethyl pyrazole analog **13** was prepared, and it exhibited favorable *in vivo* clearance coupled with excellent potency and PDE selectivity, and a favorable MDR1 efflux ratio. Unfortunately, however, the series of carbon-linked heteroaryl derivatives **10–13** were all found to possess significant *in vitro* phototoxicity potential, as evidenced by the large reduction in the viability of cells exposed to the compounds in the presence of UV radiation, relative to that in the absence of UV.⁴⁶⁾ Although the incidence of *in vivo* phototoxicity depends on drug distribution to light-exposed tissues like the skin and eye, it is generally recognized that reducing the *in vitro* phototoxicity potential of drug candidates during the lead-optimization process is a prudent strategy to minimize the potential risk for *in vivo* phototox-

icity in animals and humans. A phototoxicity liability could impose significant limitations in a drug clinical use, including the requirement to avoid sun exposure by means of sunscreen, protective clothing, and eyewear.^{47,48)} We therefore sought to minimize the *in vitro* phototoxicity liability observed in this compound series. With the hope of altering the electronic nature of the core, thus lowering the risk of *in vitro* phototoxicity, nitrogen-linked heteroaryl groups were explored. Installation of a pyrazole at the 5-position of the core to obtain **14**, a regioisomer of **13**, resulted in moderately decreased potency and PDE selectivity, but a favorable MDR1 efflux ratio and *in vivo* clearance. Of particular note was the fact that **14** showed greatly improved phototoxic liability. This encouraging result prompted us to synthesize the structurally related imidazole analog **15**. The compound exhibited improved potency and PDE selectivity with no appreciable *in vitro* phototoxicity potential, but was found to be susceptible to P-gp mediated efflux, most likely due to the polar or basic nitrogen atom of the imidazole ring.^{44,45)} In order to attenuate the basicity of the imidazole ring in **15**, a two-pronged approach was implemented: first, the methyl group on the imidazole ring was replaced with an electron-withdrawing trifluoromethyl group to give **16**, and second, an additional nitrogen atom was incorporated into the imidazole ring to afford two isomeric triazoles **17** and **18**. As anticipated, all modifications improved the P-gp efflux ratio, and maintained favorable clearance and *in vitro* phototoxicity profile, although the result of the phototoxicity

assay of compound **17** was inconclusive due to its precipitation at the concentration tested, 50 μM . Despite these benefits, both compounds showed a concomitant 5- to 10-fold loss in potency, in addition to a decrease in PDE selectivity. Overall, substitutions at the 5-position of the pyrazolo[1,5-*a*]pyrimidine core did not result in analogs with aligned potency, PDE selectivity, and other preclinical properties.

In an attempt to rescue insufficient potency and PDE selectivity of compounds **17** and **18**, which were otherwise close to meeting our goals, the methyl substitution at the 6-position of the pyrazolo[1,5-*a*]pyrimidine core was examined (**19**, **20** in Table 2), since the 6-methyl substitution was previously shown to significantly enhance both potency and PDE selectivity.⁴²⁾ In good agreement with the previous findings, introducing the methyl group at the 6-position of the pyrazolo[1,5-*a*]pyrimidine core of **17** and **18** to provide **19** and **20**, respectively, demonstrated a substantial improvement of potency and PDE selectivity (see Table 3 for inhibitory activity profile against each PDE family), without compromising MDR1 efflux ratios and *in vitro* phototoxicity risks. The phototoxic potential of compound **19** was not accurately assessed due to its low aqueous solubility, with precipitation observed at 50 μM as in the case of **17**. It appears certain, however, that its phototoxic potential was considerably lower than those of carbon-linked heteroaryl derivatives such as **10**–**13**. This is because compound **19** showed no signs of phototoxicity liability at 25 μM where no precipitate occurred, while carbon-linked derivatives **10**–**13** all displayed significant levels of UV-induced cytotoxicity at the same concentration (data not shown). It is also worth noting that plasma clearance of **19** and **20** in rat was significantly improved compared with that of **6**, which

lacks the substituent at the 5-position. Metabolite identification studies on **6** with human and rat hepatocytes revealed a single metabolite common to both species, and also indicated the 6-methyl group of the core to be the most likely site of oxidative metabolism. Based on these results, it was speculated that the triazole rings in **19** and **20** may contribute to attenuation of oxidative metabolism of the methyl groups through steric shielding effects. In the meantime, further profiling of physicochemical properties of both compounds demonstrated that **19** had extremely poor aqueous solubility that could lead to non-linear oral absorption, while **20** was approximately 10-fold more soluble with high degree of crystallinity similar to **19** (Table 4). These results are consistent with the solubility issue identified in the *in vitro* phototoxicity assay. Consequently, compound **20** was advanced to further characterization by an X-ray co-crystallization analysis as well as a series of *in vivo* studies.

The X-ray co-crystal structure of **20** bound to the catalytic domain of the PDE2A enzyme is presented in Fig. 6A and that of **7** in Fig. 6B. Compound **20** retains a number of key interactions observed in the case of the first generation lead **7**,⁴²⁾ including (i) a C–H hydrogen bonding interaction of the pyrazolo[1,5-*a*]pyrimidine core with the carbonyl oxygen atom of Gln859, (ii) π – π and CH– π interactions of the core with the Phe862 and Ile826 located above and below the core, respectively, (iii) van der Waals interactions of the 6-methyl group of the core with a hydrophobic cavity surrounded by Tyr827, Leu858, and Met847, (iv) interactions of the amide carbonyl group with two water molecules, one of which serves as a bridging water molecule to interact with the OH of Tyr655 (these interactions are not shown in the figure for simplicity), and (v) hydrophobic interactions of the RHS trifluoromethoxyphenyl group with the hydrophobic pocket newly formed due to ligand binding. In addition to the above conserved interactions, new ones characteristic of **20** that may greatly contribute to the potency enhancement are observed. The triazole ring incorporated into the 5-position of the core effectively fills the space sandwiched between Ile866 on the top and Met847 on the bottom, thus making favorable van der Waals interactions. It appears that a hydrogen bond between the triazole nitrogen atom with a bridging water molecule and the

Table 4. Thermodynamic Solubility of Compounds **19** and **20**

Compd.	Thermodynamic solubility ($\mu\text{g/mL}$)			Crystallinity (%)
	pH 1.2	pH 6.8	pH 6.8+GCDC ^{a)}	
19	0.45	0.32	16	89
20	7	4.1	140	83

^{a)} Solubility in a pH 6.8 solution containing sodium glycochenodeoxycholate (GCDC). This is considered as simulated intestinal fluid (pH 6.8) in the presence of bile acid.

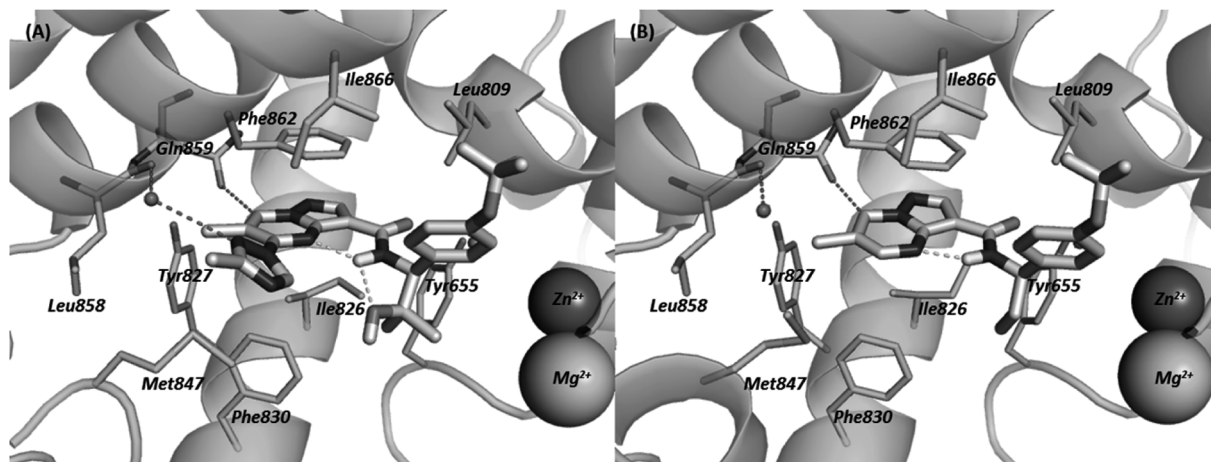


Fig. 6. (A) X-Ray Crystal Structure of **20** Bound in the PDE2A Catalytic Site (PDB 5VP1) and (B) X-Ray Crystal Structure of **7** Bound in the PDE2A Catalytic Site (PDB 5XKM)

The intramolecular hydrogen bonds are indicated by light dotted lines.

backbone carbonyl group of Leu858 may have some positive impacts on the potency. Furthermore, the branched tertiary alcohol moiety would serve to provide greater conformational rigidity to the molecule through not only an intramolecular hydrogen bond between the oxygen atom of the tertiary alcohol and the amide NH, but also restriction of the bond rotation imparted by the *gem*-dimethyl group, and thereby offer a benefit with reduced entropic cost of binding by biasing the RHS benzylamine moiety toward the bioactive conformation.

The preclinical pharmacokinetic (PK) profiles of compound **20** in rat and mouse are summarized in Table 5. Compound **20** exhibited favorable PK parameters in both rat and mouse, characterized by reduced plasma clearance and moderate oral bioavailability. In addition, the compound demonstrated reasonable brain uptake with a brain to plasma ratio of 0.32 in rat, although it had a high TPSA value (114 Å²) outside the traditional range of CNS drugs.^{44,45,49} These results suggested that the intramolecular hydrogen bonds observed in **20** effectively shield the polarity of the molecule, thus improving blood-brain barrier permeability.

In order to assess target engagement, the dose–occupancy relationship of compound **20** was characterized by measuring PDE2A occupancy 2 h after oral administration of five escalating doses: 0.3, 1, 3, 10, and 30 mg/kg. As shown in Fig. 7, compound **20** dose-dependently occupied PDE2A in rat striatum with a 50% target occupancy oral dose (ED₅₀) of 3.9 mg/kg. Based on these results, cyclic nucleotide levels in the frontal cortex, hippocampus, and striatum of rat brain,

Table 5. PK Parameters and K_p Values of Compound **20** in Rats and Mice^{a)}

	Rat	Mouse
CL_{total}^b (mL/h/kg)	1169.0	768.0
Vd_{ss}^c (mL/kg)	2329.0	1337.0
C_{max}^d (ng/mL)	58.1	181.0
T_{max}^e (h)	2.0	0.7
AUC_{0-8h}^f (ng·h/mL)	272.8	628.6
F^g (%)	31.2	48.2
K_p^h	0.32	—

a) Cassette dosing at 0.1 mg/kg, i.v. and 1 mg/kg, p.o. (non-fasted), in an average of 3 rats or mice. b) Total clearance. c) Volume of distribution at steady state. d) Maximum plasma concentration. e) Time of maximum concentration. f) Area under the plasma concentration vs. time curve (0–8 h). g) Oral bioavailability. h) Brain-to-plasma ratio at 2 h after oral administration of **20** at a dose of 10 mg/kg.

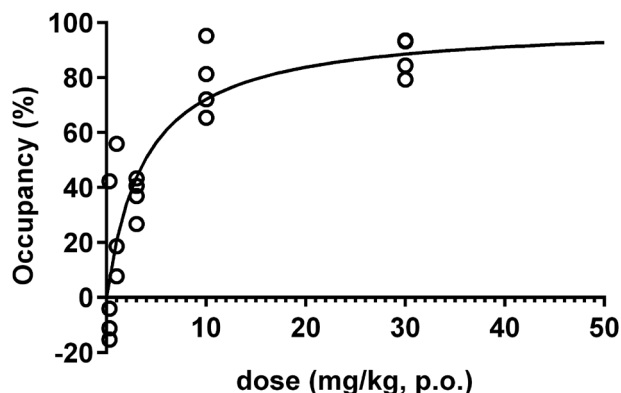


Fig. 7. *In Vivo* PDE2A Target Occupancy in the Striatum Measured 2 h after Oral Administration of **20** in Rats

where the PDE2A enzyme is highly expressed,^{13–18}) were measured to assess the PD effects of compound **20** (Fig. 8). Consistent with the previous observations,^{11,29,42,43,50} compound **20** dose-dependently increased cGMP levels in all selected brain regions at doses as low as 3 mg/kg, corresponding to *ca.* 37% occupancy levels, while not affecting cAMP levels. These results suggest that oral administration of **20** at doses of 3 mg/kg or above would lead to significant pharmacological effects in preclinical models of cognition. We therefore performed a passive avoidance test in MK-801-treated rats to evaluate the effects of **20** at an oral dose of 3 mg/kg on deficits in episodic memory induced by *N*-methyl-D-aspartate (NMDA) receptor hypofunction^{51,52} (Fig. 9). Subcutaneous administration of MK-801 at 0.1 mg/kg significantly decreased the avoidance time in the retention test, compared to saline treatment ($p \leq 0.01$). Pretreatment with 3 mg/kg of **20** significantly attenuated the decrease in the avoidance time induced by MK-801 ($p \leq 0.01$). The ability of **20** to reverse deficits in episodic memory produced by MK-801, suggests its potential for the treatment of cognitive deficits seen in a range of psychiatric disorders with impaired glutamatergic neurotransmission.

Chemistry The RHS benzylamine moiety **28** was prepared as outlined in Chart 1. Benzaldehyde **21** was initially converted to the corresponding hydantoin **22** using the Bucher–Berger reaction.⁵³ Hydantoin **22** was then hydrolyzed

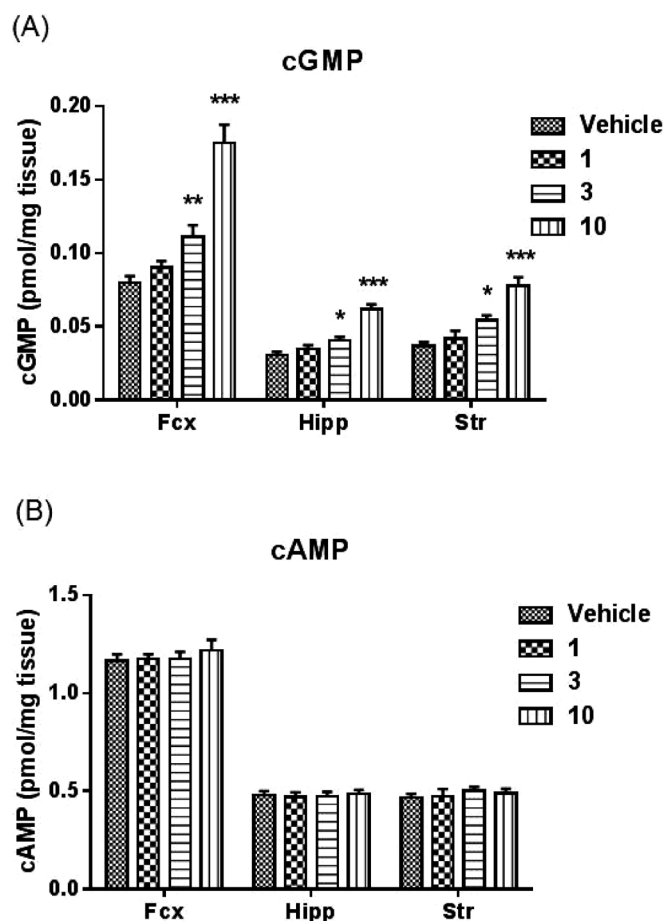


Fig. 8. Effects of Compound **20** on Cyclic Nucleotides in Rat Brain

cGMP (A) and cAMP (B) levels 2 h after oral administration of compound **20** (1, 3, 10 mg/kg) were measured in the rat frontal cortex (Fcx), hippocampus (Hipp), and striatum (Str). Data are presented as mean \pm S.E.M. ($n=9$). * $p < 0.025$, ** $p < 0.005$, *** $p < 0.0005$, vs. vehicle by Shirley–Williams' test.

under basic conditions to afford amino acid **23**. The protection of the amino group of **23** with a Boc group using Schotten–Baumann conditions and subsequent methylation of the carboxylic acid **24** gave methyl ester **25**. Treatment of **25** with methyl Grignard reagent, followed by chiral separation provided enantiomers **27a** and **b**. Finally, the Boc group of the

desired enantiomer **27a** was removed under acidic conditions to give RHS benzylamine **28** as a hydrochloride salt.

A series of 5-substituted pyrazolo[1,5-*a*]pyrimidine derivatives **8–18** were prepared following the procedures depicted in Chart 2. Starting from elaboration of the pyrazolopyrimidine core **30** by the condensation of 5-amino-1*H*-pyrazole **29** with a mixture of *cis*- and *trans*-ethyl 3-ethoxyacrylate under basic conditions, the ethyl ester of **30** was hydrolyzed to afford carboxylic acid **31**. Bischlorination of **31** with phosphoryl chloride (POCl_3) gave **32**, which was subsequently reacted with RHS benzylamine **28**, to furnish 5-chloropyrazolo[1,5-*a*]pyrimidine **33**. Attachment of the substituent at the 5-position of the pyrazolo[1,5-*a*]pyrimidine core was finally accomplished by the following three approaches: i) Suzuki–Miyaura cross-coupling of the corresponding boronic acids or esters to deliver **11–13**; ii) Suzuki–Miyaura cross-coupling followed by catalytic hydrogenation of the olefin moieties to deliver **8** and **9**; and iii) nucleophilic displacement with the corresponding azoles to deliver **14–18**. However, Suzuki–Miyaura cross-coupling employing **33** to obtain 2-pyridyl derivative **10** was unsuccessful, probably due to the relatively unstable nature of 2-pyridylboron species as well as the presence of polar functionalities such as the amide and the tertiary alcohol moieties in **33** that could potentially coordinate with the palladium catalyst. Therefore, attempts were made to introduce the 2-pyridyl group at the early step prior to the amide coupling with the RHS benzylamine moiety. After chlorination of **30** with POCl_3 , 5-chloropyrazolo[1,5-*a*]pyrimidine **36** was successfully coupled with lithium 2-pyridyltriolborate salt **37** via Suzuki–Miyaura cross-coupling catalyzed by palladium(II) acetate and triphenylphosphine (Ph_3P) in the presence of copper(I)

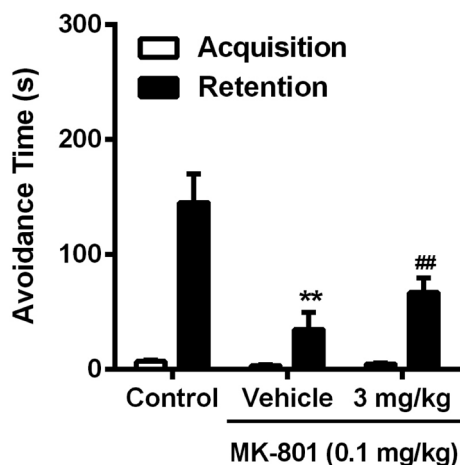
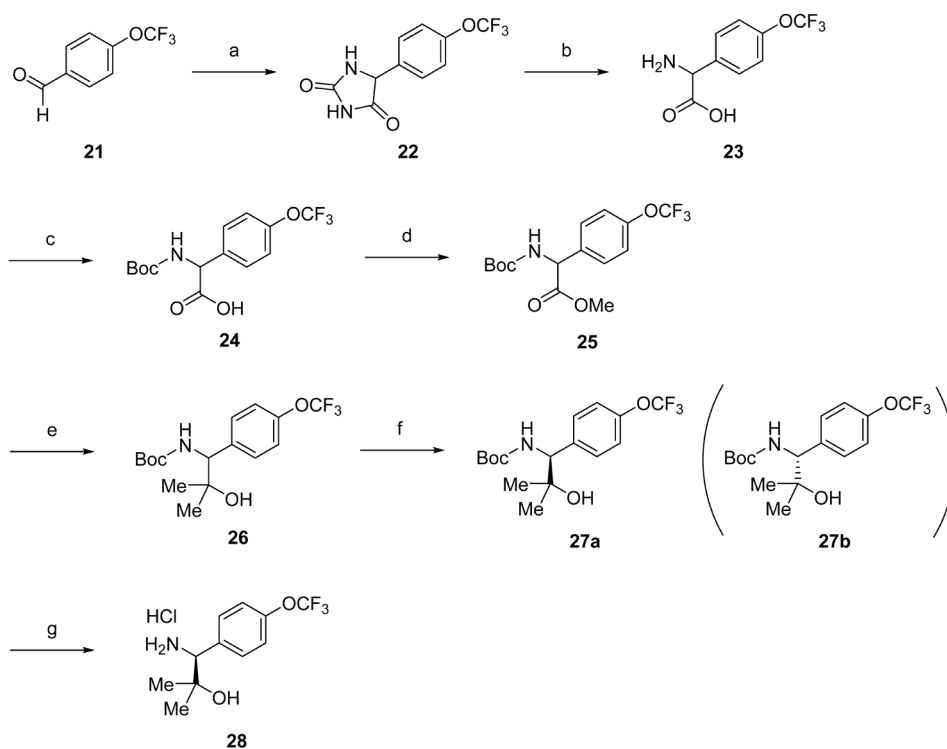


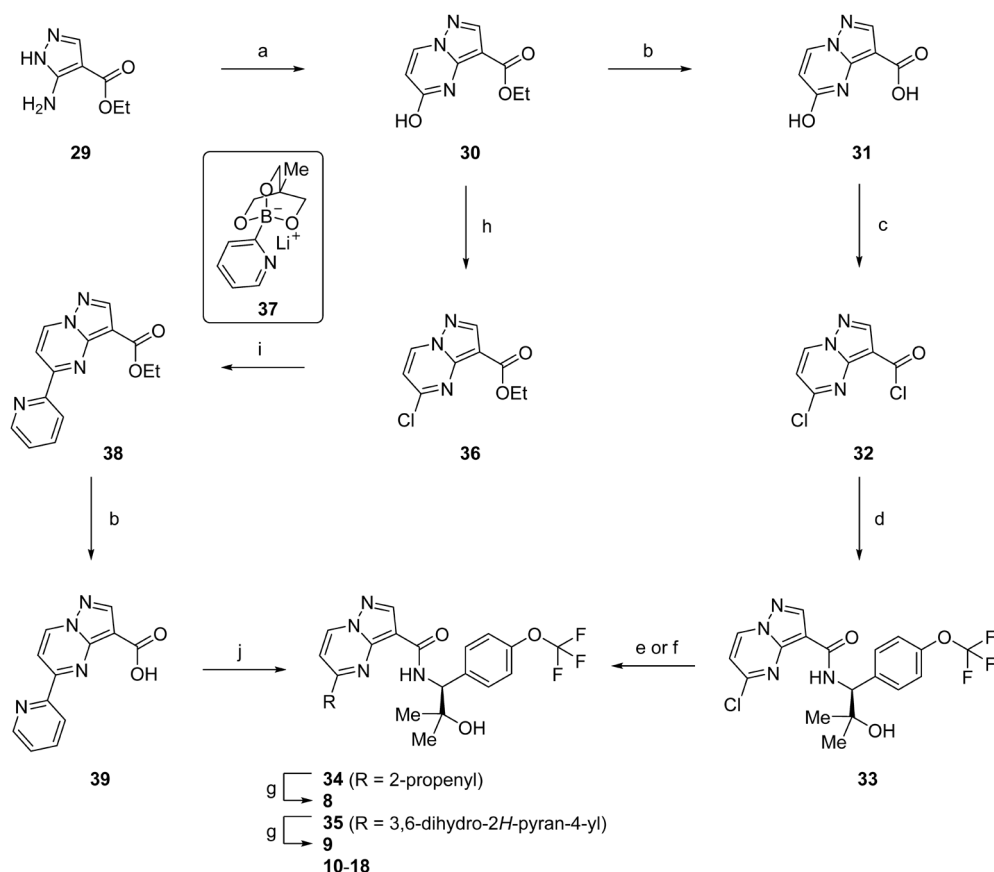
Fig. 9. Effects of Compound **20** on MK-801-Induced Episodic Memory Deficits Assessed by the Passive Avoidance Task in Rats

Vehicle or compound **20** (3 mg/kg) was orally administered 90 min before the s.c. administration of saline or MK-801. Thirty minutes after the s.c. administration of saline or MK-801 (0.1 mg/kg), the rat was placed on the illuminated chamber. The latency to cross over into the dark chamber was recorded for up to a maximum of 300 s. The retention test was carried out 24 h after the acquisition trial. Data (latency to cross over into the dark compartment on the retention trial) are expressed as mean \pm S.E.M., $n=20$. ** $p \leq 0.01$ (versus control by Wilcoxon's test), ## $p \leq 0.01$ (versus vehicle+MK-801 by Wilcoxon's test).



Reagents and conditions: (a) KCN, $(\text{NH}_4)_2\text{CO}_3$, EtOH, H_2O , 50 to 60°C, 3 h, (taken on crude); (b) KOH, water, 90°C, 3 d, (taken on crude); (c) Boc_2O , 2M NaOH aq., THF, r.t., overnight, (taken on crude); (d) MeI, K_2CO_3 , DMF, r.t., 2 h, 46% (4 steps from **21**); (e) MeMgBr, THF, 0°C, 1 h, 76%; (f) Chiralpak AD, hexane–EtOH=19:1; (g) HCl, EtOAc, r.t., 1.5 h, 84%.

Chart 1. Synthesis of RHS Benzylamine Moiety **28**



Reagents and conditions: (a) ethyl 3-ethoxyacrylate (*cis*- and *trans*-mixture), Cs_2CO_3 , DMF, 100°C, 2 h, 91%; (b) NaOH aq., THF, EtOH, 50–60°C, 2 h–overnight, 75–98%; (c) POCl_3 , DIEA, 130°C, 4 h, 74%; (d) RHS benzylamine **28**, DIEA, CH_3CN , 0°C to r.t., 16 h, 77%; (e) alkyl or arylboronic acid pinacolester, (Amphos) $_2\text{PdCl}_2$, K_2CO_3 , toluene, H_2O , 120–150°C (microwave), 25 min–2.5 h, 63–78%; (f) azole, K_2CO_3 , DMF, 80–90°C, 30 min–2 h, 7–74%; (g) H_2 , 5% Pd/C–ethylenediamine complex, MeOH, r.t., 16 h, 83–98%; (h) POCl_3 , 100°C, 16 h, 61%; (i) lithium 4-methyl-1-pyridin-2-yl-2,6,7-trioxa-1-borabicyclo[2.2.2]octan-1-uide **37**, $\text{Pd}(\text{OAc})_2$, Ph_3P , CuI, DMF, 80°C, 2 h, 87%; (j) RHS benzylamine **28**, HATU, DIEA, DMF, r.t., 12 h, 84%.

Chart 2. Synthesis of 5-Substituted Pyrazolo[1,5-*a*]pyrimidine Derivatives **8–18**

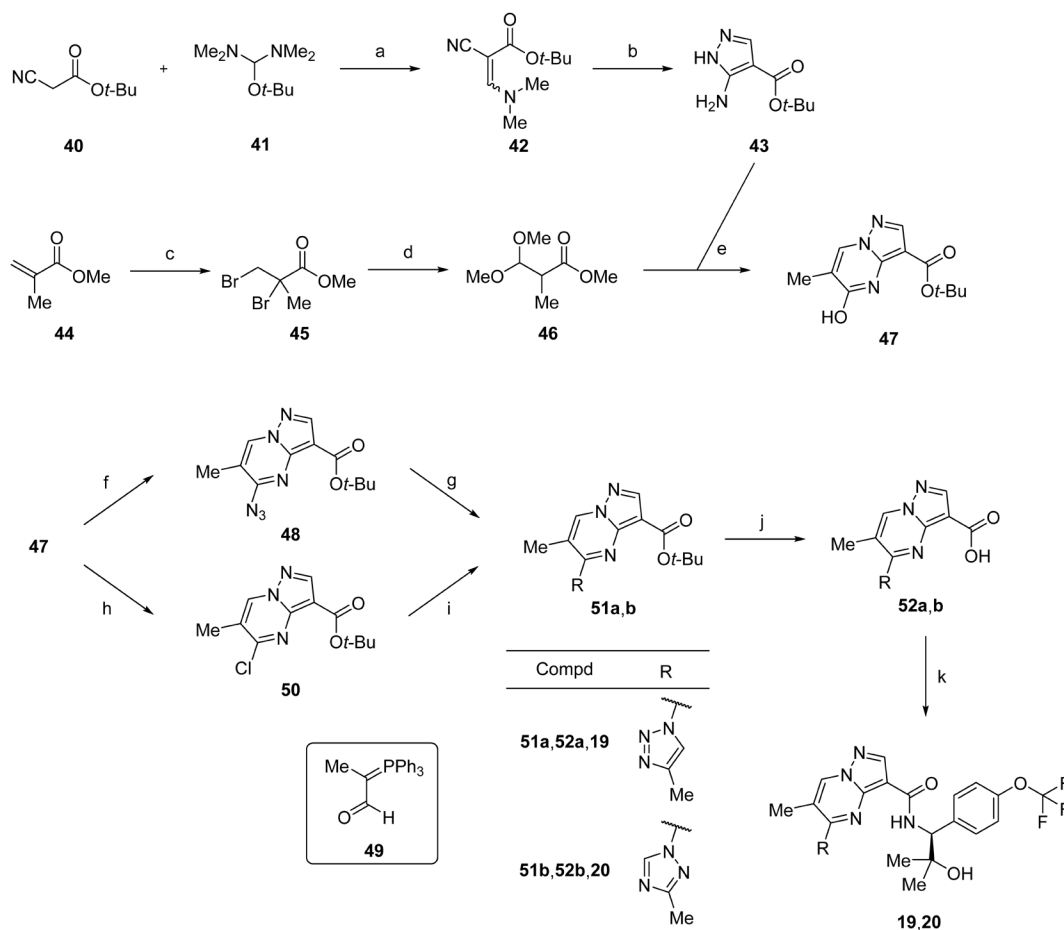
iodide,⁵⁴) providing coupled product **38**. Ester hydrolysis of **38** and subsequent amide formation with RHS benzylamine **28** furnished the final compound **10**.

The synthetic route to access compounds **19** and **20** is highlighted in Chart 3. Aminopyrazole **43** was initially constructed in a two-step sequence of reactions, involving the condensation of *tert*-butyl 2-cyanoacetate (**40**) and *tert*-butoxy bis(dimethylamino)methane (**41**), followed by reaction with hydrazine. The aminopyrazole **43** was then condensed with 1,3-dicarbonyl related electrophile **46** prepared by bromination of methyl methacrylate (**44**), prior to treatment with a methanol solution of sodium methoxide to provide pyrazolo[1,5-*a*]pyrimidine core **47**. Regioselective installation of triazole rings at the 5-position of the core was carried out by two different approaches using conditions mild enough to be compatible with the acid-labile *tert*-butyl ester moiety. One approach involved diphenylphosphoryl azide (DPPA)-mediated azidation prior to the regioselective 1,3-dipolar cycloaddition of the resulting azido group of **48** to the C=C bond of the betainic form of α -formylethylidene-triphenylphosphorane (**49**) with subsequent spontaneous elimination of triphenylphosphine oxide,^{55,56}) to deliver **51a**. The other involved Appel-type chlorination with carbon tetrachloride (CCl_4) and PPh_3 , followed by $\text{S}_\text{N}\text{Ar}$ displacement with 3-methyl-1*H*-1,2,4-triazole to afford **51b** in a regioselective manner. The resulting *tert*-butyl esters **51a, b** were hydrolyzed under acidic conditions

to give the corresponding carboxylic acids **52a, b**, which were finally coupled with benzylamine **28** to afford amide products **19** and **20**.

Conclusion

In summary, a new class of PDE2A inhibitors, structurally different from our clinical candidate TAK-915 were identified by incorporating features from our previously reported PDE2A inhibitor series such as **3** and **4**. With an initial goal of enhancing the potency of new lead compound **5**, substitutions on the pyrazolo[1,5-*a*]pyrimidine core, especially at the 5- and 6-positions, were explored on the basis of previous SAR knowledge and crystal structure information of pyrazolo[1,5-*a*]pyrimidine analog **7**. Our optimization efforts resulted in the discovery of *N*-((1*S*)-2-hydroxy-2-methyl-1-(4-(trifluoromethoxy)phenyl)propyl)-6-methyl-5-(3-methyl-1*H*-1,2,4-triazol-1-yl)-pyrazolo[1,5-*a*]pyrimidine-3-carboxamide (**20**), a potent brain-penetrating PDE2A inhibitor highly selective over other PDE families. Introduction of a nitrogen-linked heteroaryl substituent at the 5-position as in **20** was key to alleviating *in vitro* phototoxicity risk. In addition, despite its high TPSA value (114 Å²) which is beyond the optimal range for CNS drugs, compound **20** exhibited acceptable brain exposure probably due to cloaking of HBD and HBA groups *via* intramolecular hydrogen bonding. This was also supported by an X-ray crystal structure of **20** bound to PDE2A. In the subse-



Reagents and conditions: (a) neat, r.t., 30 min (taken on crude); (b) $\text{NH}_2\text{NH}_2 \cdot \text{H}_2\text{O}$, MeOH, 70°C, overnight, 64%; (c) Br_2 , EtOAc, r.t., 16 h, (taken on crude); (d) NaOMe, MeOH, 70°C, 3 h, (taken on crude); (e) Cs_2CO_3 , DMF, 100°C, 16 h, 84%; (f) DPPA, DBU, THF, 60°C, 5 h, 74%; (g) **49**, toluene, 80°C, 3 h, then MgCl_2 , 60°C, 2 h, 97%; (h) CCl_4 , PPh_3 , 1,2-dichloroethane, 75–85°C, 4.5 h, 88%; (i) 3-methyl-1*H*-1,2,4-triazole, K_2CO_3 , DMF, 60°C, 2 h, 69%; (j) MsOH, CH_3CN , r.t.–60°C, 5.5 h–overnight, 85–91%; (k) RHS benzylamine **28**, EDCI·HCl, HOBT· H_2O , Et_3N , DMF, r.t., 2 h–overnight, 75–82%.

Chart 3. Synthesis of 6-Methyl-5-Substituted Pyrazolo[1,5-*a*]pyrimidine Derivatives **19** and **20**

quent *in vivo* studies on **20**, we confirmed dose-dependent target engagement in rat brain after oral dosing. Correlated with these results, compound **20** exhibited dose-dependent increases in cGMP levels in the brain and, moreover, improved cognitive function in a rat model of schizophrenia following oral administration at the dose where PD effects were noted. Thus, potent and selective PDE2A inhibitors, such as compound **20**, are hypothesized to provide a novel therapeutic approach to treat cognitive dysfunction in a range of neuropsychiatric and neurodegenerative disorders, including schizophrenia and Alzheimer's disease.

Experimental

General Chemistry Information All solvents and reagents were obtained from commercial sources and were used as received. Microwave-assisted reactions were carried out in a single-mode reactor, Biotage Initiator 2.0 or 2.5 microwave synthesizer. Yields were not optimized. All reactions were monitored by TLC analysis on Merck Kieselgel 60 F254 plates or Fuji Silysia NH plates, or LC-MS analysis. LC-MS analysis was performed on a Shimadzu LC-MS system operating in atmospheric pressure chemical ionization (APCI) (+ or –) or electrospray ionization (ESI) (+ or –) ionization mode. Analytes were eluted using a linear gradient with a mobile phase of water/acetonitrile containing 0.05% trifluoroacetic acid

(TFA) or 5 mM ammonium acetate and detected at 220 nm. Column chromatography was carried out on silica gel ((Merck Kieselgel 60, 70–230 mesh, Merck) or (Chromatorex NH-DM 1020, 100–200 mesh, Fuji Silysia Chemical, Ltd.)), or on pre-packed Purif-Pack columns (SI or NH, particle size: 60 μm , Fuji Silysia Chemical, Ltd.). Analytical HPLC was performed using a Corona Charged Aerosol Detector or photo diode array detector with a Capcell Pak C18AQ (3.0 mm ID×50 mm L, Shiseido, Japan) or L-column2 ODS (2.0 mm ID×30 mm L, CERI, Japan) column at a temperature of 50°C and a flow rate of 0.5 mL/min. Mobile phases A and B under neutral conditions were a mixture of 50 mmol/L ammonium acetate, water, and acetonitrile (1:8:1, v/v/v) and a mixture of 50 mmol/L ammonium acetate and acetonitrile (1:9, v/v), respectively. The ratio of mobile phase B was increased linearly from 5 to 95% over 3 min, and then maintained at 95% over the next 1 min. Mobile phases A and B under acidic conditions were a mixture of 0.2% formic acid in 10 mmol/L ammonium formate and 0.2% formic acid in acetonitrile, respectively. The ratio of mobile phase B was increased linearly from 14 to 86% over 3 min, and then maintained at 86% over the next 1 min. All final test compounds were purified to >95% chemical purity as measured by analytical HPLC. Elemental analyses were carried out by Takeda Analytical Laboratories, and all results were within $\pm 0.4\%$ of the theoretical values. Melting

points were determined on a BÜCHI B-545 melting point apparatus or a DSC1 system (Mettler-Toledo International Inc., Greifensee, Switzerland). Proton nuclear magnetic resonance ($^1\text{H-NMR}$) spectra were recorded on a Varian Mercury-300 (300MHz) or Bruker DPX300 (300MHz) instrument. All $^1\text{H-NMR}$ spectra were consistent with the proposed structures. All proton shifts are given in parts per million (ppm) downfield from tetramethylsilane (δ) as the internal standard in deuterated solvent, and coupling constants (J) are in hertz (Hz). NMR data are reported as follows: chemical shift, integration, multiplicity (s, singlet; d, doublet; t, triplet; q, quartet; quint, quintet; m, multiplet; dd, doublet of doublets; td, triplet of doublets; ddd, doublet of doublet of doublets; and brs, broad singlet), and coupling constants. Very broad peaks for protons of, for example, hydroxyl and amino groups are not always indicated.

***N*-((1*S*)-2-Hydroxy-2-methyl-1-(4-(trifluoromethoxy)phenyl)propyl)-5-isopropylpyrazolo[1,5-*a*]pyrimidine-3-carboxamide (8)** A mixture of **34** (38.6 mg, 0.09 mmol) and 5% Pd/C–ethylenediamine complex (10 mg) in MeOH (5 mL) was hydrogenated under balloon pressure at room temperature (r.t.) for 16 h. The catalyst was removed by filtration and the filtrate was concentrated *in vacuo*. The residue was purified by column chromatography (silica gel, hexane–ethyl acetate, 19:1 to 0:100) to afford **8** (32.1 mg, 0.074 mmol, 83%) as a white amorphous solid. $^1\text{H-NMR}$ (300 MHz, DMSO- d_6) δ : 0.99–1.08 (3H, m), 1.27 (3H, s), 1.41 (3H, d, $J=4.5$ Hz), 1.43 (3H, d, $J=4.5$ Hz), 3.20–3.34 (1H, m), 4.81–5.00 (2H, m), 7.22–7.34 (3H, m), 7.48–7.61 (2H, m), 8.44 (1H, s), 9.07 (1H, d, $J=8.7$ Hz), 9.19 (1H, d, $J=7.2$ Hz). MS (ESI/APCI) m/z 437.1 $[\text{M}+\text{H}]^+$. HPLC purity: 98.9%.

***N*-((1*S*)-2-Hydroxy-2-methyl-1-(4-(trifluoromethoxy)phenyl)propyl)-5-(tetrahydro-2*H*-pyran-4-yl)pyrazolo[1,5-*a*]pyrimidine-3-carboxamide (9)** A mixture of **35** (84.4 mg, 0.177 mmol) and Pd/C (en) (15 mg) in MeOH (10 mL) and tetrahydrofuran (THF) (dry) (2 mL) was hydrogenated under balloon pressure at r.t. for 16 h. The catalyst was removed by filtration and the filtrate was concentrated *in vacuo*. The residue was purified by column chromatography (silica gel, hexane–ethyl acetate, 19:1 to 0:100) to afford **9** (82.9 mg, 0.173 mmol, 98%) as a white amorphous solid. $^1\text{H-NMR}$ (300 MHz, DMSO- d_6) δ : 1.04 (3H, s), 1.28 (3H, s), 1.86–2.11 (4H, m), 3.13–3.28 (1H, m), 3.45–3.59 (2H, m), 3.97–4.10 (2H, m), 4.88–4.99 (2H, m), 7.24–7.34 (3H, m), 7.50–7.61 (2H, m), 8.45 (1H, s), 9.03 (1H, d, $J=8.7$ Hz), 9.21 (1H, d, $J=7.2$ Hz). MS (ESI/APCI) m/z 479.1 $[\text{M}+\text{H}]^+$. HPLC purity: 99.6%.

***N*-((1*S*)-2-Hydroxy-2-methyl-1-(4-(trifluoromethoxy)phenyl)propyl)-5-(pyridin-2-yl)pyrazolo[1,5-*a*]pyrimidine-3-carboxamide (10)** A mixture of crude **39** (79.0 mg, 0.329 mmol), **28** (94.0 mg, 0.329 mmol), HATU (163 mg, 0.428 mmol), *N,N*-diisopropylethylamine (DIEA) (0.172 mL, 0.987 mmol), and *N,N*-dimethylformamide (DMF) (3 mL) was stirred at r.t. for 12 h. The mixture was diluted with water and extracted with EtOAc. The organic layer was separated, washed with saturated aqueous NaCl, dried over anhydrous Na_2SO_4 and concentrated *in vacuo*. The residue was purified by column chromatography (basic silica gel, hexane–ethyl acetate, 100:0 to 0:100) to give **10** (130 mg, 0.276 mmol, 84% (63% yield in 2 steps from **39**)) as a pale yellow amorphous solid. $^1\text{H-NMR}$ (300 MHz, CDCl_3) δ : 1.21 (3H, s), 1.49 (3H, s), 1.96 (1H, s), 5.14 (1H, d, $J=8.3$ Hz), 7.14–7.22 (2H, m),

7.44–7.56 (3H, m), 7.88–7.97 (1H, m), 8.26 (1H, d, $J=7.4$ Hz), 8.64 (1H, s), 8.75–8.88 (3H, m), 9.25 (1H, d, $J=8.3$ Hz). MS (ESI/APCI) m/z 472.1 $[\text{M}+\text{H}]^+$. HPLC purity: 97.3%. *Anal.* Calcd for $\text{C}_{23}\text{H}_{20}\text{F}_3\text{N}_5\text{O}_3$: C, 58.60; H, 4.28; N, 14.86. Found: C, 58.61; H, 4.51; N, 14.86.

***N*-((1*S*)-2-Hydroxy-2-methyl-1-(4-(trifluoromethoxy)phenyl)propyl)-5-(6-methylpyridin-3-yl)pyrazolo[1,5-*a*]pyrimidine-3-carboxamide (11)** The title compound was prepared as a pale yellow solid after trituration with hexane–ethyl acetate (5:1) in 63% yield from **33** and 2-methyl-5-(4,4,5,5-tetramethyl-1,3,2-dioxaborolan-2-yl)pyridine using the procedure analogous to that described for the synthesis of **35**, except that basic silica gel was employed in a column chromatography purification in place of silica gel. $^1\text{H-NMR}$ (300 MHz, DMSO- d_6) δ : 1.03 (3H, s), 1.33 (3H, s), 2.60 (3H, s), 4.93 (1H, d, $J=8.3$ Hz), 5.19 (1H, s), 7.23–7.33 (2H, m), 7.48–7.59 (3H, m), 7.98 (1H, d, $J=7.5$ Hz), 8.50 (1H, s), 8.81 (1H, dd, $J=8.3, 2.3$ Hz), 9.24 (1H, d, $J=8.7$ Hz), 9.41 (1H, d, $J=7.5$ Hz), 9.54 (1H, d, $J=2.3$ Hz). MS (ESI/APCI) m/z 486.1 $[\text{M}+\text{H}]^+$. HPLC purity: 100%. mp 237°C.

***N*-((1*S*)-2-Hydroxy-2-methyl-1-(4-(trifluoromethoxy)phenyl)propyl)-5-(2-methylpyridin-4-yl)pyrazolo[1,5-*a*]pyrimidine-3-carboxamide (12)** A mixture of **33** (130 mg, 0.303 mmol), 2-methyl-4-(4,4,5,5-tetramethyl-1,3,2-dioxaborolan-2-yl)pyridine (100 mg, 0.455 mmol), (Amphos) $_2$ PdCl $_2$ (21.5 mg, 0.0303 mmol), K_2CO_3 (62.9 mg, 0.455 mmol), toluene (2 mL) and water (0.2 mL) was heated at 120°C under microwave irradiation for 2.5 h. After being cooled to r.t., the reaction mixture was directly purified by column chromatography (basic silica gel, ethyl acetate–methanol, 100:0 to 19:1) to give **12** (115 mg, 0.237 mmol, 78%) as an off-white solid after recrystallization from heptane–ethyl acetate. $^1\text{H-NMR}$ (300 MHz, CDCl_3) δ : 1.21 (3H, s), 1.50 (3H, s), 1.73 (1H, s), 2.72 (3H, s), 5.13 (1H, d, $J=8.5$ Hz), 7.13–7.20 (2H, m), 7.46–7.54 (3H, m), 7.91 (1H, dd, $J=5.1, 1.3$ Hz), 8.09 (1H, s), 8.67 (1H, s), 8.75 (1H, d, $J=5.3$ Hz), 8.88 (1H, d, $J=7.4$ Hz), 9.19 (1H, d, $J=8.3$ Hz). MS (ESI/APCI) m/z 486.1 $[\text{M}+\text{H}]^+$. HPLC purity: 100%. mp 192°C. *Anal.* Calcd for $\text{C}_{24}\text{H}_{22}\text{F}_3\text{N}_5\text{O}_3$: C, 59.38; H, 4.57; N, 14.43. Found: C, 59.03; H, 4.60; N, 14.24.

5-(1-(Difluoromethyl)-1*H*-pyrazol-4-yl)-*N*-((1*S*)-2-hydroxy-2-methyl-1-(4-(trifluoromethoxy)phenyl)propyl)-pyrazolo[1,5-*a*]pyrimidine-3-carboxamide (13) The title compound was prepared as a white amorphous solid in 77% yield from **33** and 1-(difluoromethyl)-4-(4,4,5,5-tetramethyl-1,3,2-dioxaborolan-2-yl)-1*H*-pyrazole using the procedure analogous to that described for the synthesis of **35**, except that the crude material was purified by basic silica gel column chromatography followed by silica gel column chromatography. $^1\text{H-NMR}$ (300 MHz, DMSO- d_6) δ : 1.04 (3H, s), 1.36 (3H, s), 4.89 (1H, d, $J=8.3$ Hz), 5.28 (1H, s), 7.23–7.35 (2H, m), 7.49–7.59 (2H, m), 7.73 (1H, d, $J=7.5$ Hz), 7.97 (1H, t, $J=59.0$ Hz), 8.45 (1H, s), 8.81 (1H, s), 9.29 (1H, s), 9.32–9.42 (2H, m). MS (ESI/APCI) m/z 511.1 $[\text{M}+\text{H}]^+$. HPLC purity: 100%.

***N*-((1*S*)-2-Hydroxy-2-methyl-1-(4-(trifluoromethoxy)phenyl)propyl)-5-(1*H*-pyrazol-1-yl)pyrazolo[1,5-*a*]pyrimidine-3-carboxamide (14)** To a mixture of **33** (126.3 mg, 0.295 mmol) and 1*H*-pyrazole (24.1 mg, 0.353 mmol) in DMF (4 mL) was added K_2CO_3 (48.8 mg, 0.353 mmol). The mixture was stirred at 90°C for 30 min and then poured into water. The mixture was extracted with EtOAc, washed with water

and saturated aqueous NaCl, dried over anhydrous Na₂SO₄ and concentrated *in vacuo*. The residue was purified by column chromatography (silica gel, hexane–ethyl acetate, 19:1 to 0:100) to afford **14** (102 mg, 0.222 mmol, 75%) as a white solid after trituration with hexane–ethyl acetate (5:1). ¹H-NMR (300 MHz, DMSO-*d*₆) δ: 1.02 (3H, s), 1.36 (3H, s), 4.86 (1H, d, *J*=8.3 Hz), 5.34 (1H, s), 6.75–6.81 (1H, m), 7.23–7.33 (2H, m), 7.48–7.58 (2H, m), 7.76 (1H, d, *J*=7.5 Hz), 8.05 (1H, d, *J*=1.5 Hz), 8.46 (1H, s), 9.02–9.14 (2H, m), 9.37 (1H, d, *J*=7.5 Hz). MS (ESI/APCI) *m/z* 461.1 [M+H]⁺. HPLC purity: 100%. mp 241°C.

***N*-(1*S*)-2-Hydroxy-2-methyl-1-(4-(trifluoromethoxy)-phenyl)propyl)-5-(4-methyl-1*H*-imidazol-1-yl)pyrazolo[1,5-*a*]pyrimidine-3-carboxamide (15)** The title compound was prepared as a pale yellow solid after trituration with hexane–ethyl acetate (5:1) in 70% yield from **33** and 4-methyl-1*H*-imidazole using the procedure analogous to that described for the synthesis of **14**, except that a preparative HPLC (column: L-Column2 ODS 20mm ID×150mm L; mobile phase A: 0.1% TFA in water; mobile phase B: 0.1% TFA in acetonitrile; flow rate: 20 mL/min) was employed in place of silica gel column chromatography. ¹H-NMR (300 MHz, DMSO-*d*₆) δ: 1.02 (3H, s), 1.35 (3H, s), 2.24 (3H, s), 4.87 (1H, d, *J*=8.3 Hz), 5.31 (1H, s), 7.24–7.33 (2H, m), 7.47–7.57 (2H, m), 7.73 (1H, d, *J*=7.9 Hz), 8.07 (1H, s), 8.45 (1H, s), 8.85 (1H, d, *J*=0.8 Hz), 9.00 (1H, d, *J*=8.3 Hz), 9.46 (1H, d, *J*=7.5 Hz). MS (ESI/APCI) *m/z* 475.1 [M+H]⁺. HPLC purity: 99.2%. mp 130°C.

***(S)*-*N*-(2-Hydroxy-2-methyl-1-(4-(trifluoromethoxy)-phenyl)propyl)-5-(4-(trifluoromethyl)-1*H*-imidazol-1-yl)pyrazolo[1,5-*a*]pyrimidine-3-carboxamide (16)** The title compound was prepared as a pale yellow solid after trituration with hexane–ethyl acetate (5:1) in 70% yield from **33** and 4-(trifluoromethyl)-1*H*-imidazole using the procedure analogous to that described for the synthesis of **14**. ¹H-NMR (300 MHz, DMSO-*d*₆) δ: 1.02 (3H, s), 1.34 (3H, s), 4.86 (1H, d, *J*=8.3 Hz), 5.36 (1H, s), 7.23–7.33 (2H, m), 7.47–7.58 (2H, m), 7.89 (1H, d, *J*=7.5 Hz), 8.53 (1H, s), 8.92–9.02 (2H, m), 9.15 (1H, s), 9.62 (1H, d, *J*=7.5 Hz). MS (ESI/APCI) *m/z* 529.1 [M+H]⁺. HPLC purity: 100%. mp 220°C.

***N*-(1*S*)-2-Hydroxy-2-methyl-1-(4-(trifluoromethoxy)-phenyl)propyl)-5-(4-methyl-1*H*-1,2,3-triazol-1-yl)pyrazolo[1,5-*a*]pyrimidine-3-carboxamide (17)** A mixture of **33** (430 mg, 1.00 mmol), 4-methyl-1*H*-1,2,3-triazole (100 mg, 1.20 mmol) and K₂CO₃ (208 mg, 1.50 mmol) in DMF (4 mL) was stirred at 80°C for 2 h. The mixture was quenched with water at r.t. and extracted with EtOAc. The organic layer was separated, washed with water and saturated aqueous NaCl, dried over anhydrous MgSO₄ and concentrated *in vacuo* (508.7 mg). The residue was purified by using preparative HPLC (column: L-Column2 ODS 20mm ID×150mm L; mobile phase A: 0.1% TFA in water; mobile phase B: 0.1% TFA in acetonitrile; flow rate: 20 mL/min). The first eluting fractions (tR1) were concentrated to dryness, and washed with saturated aqueous NaHCO₃, extracted with EtOAc. The organic layer was separated, washed with water and saturated aqueous NaCl, dried over anhydrous MgSO₄ and concentrated *in vacuo*. The residue (42.7 mg) was crystallized from hexane–ethyl acetate to give **17** (34.4 mg, 0.072 mmol, 7.2%) as a white solid. ¹H-NMR (300 MHz, DMSO-*d*₆) δ: 1.04 (3H, s), 1.37 (3H, s), 2.44 (3H, s), 4.87 (1H, d, *J*=8.3 Hz), 5.39 (1H, s), 7.23–7.34 (2H, m), 7.48–7.58 (2H, m), 7.93 (1H, d, *J*=7.5 Hz),

8.55 (1H, s), 8.88 (1H, d, *J*=0.8 Hz), 9.07 (1H, d, *J*=8.3 Hz), 9.50 (1H, d, *J*=7.5 Hz). MS (ESI/APCI) *m/z* 476.2 [M+H]⁺. HPLC purity: 99.4%. mp 260°C.

***N*-(1*S*)-2-Hydroxy-2-methyl-1-(4-(trifluoromethoxy)-phenyl)propyl)-5-(3-methyl-1*H*-1,2,4-triazol-1-yl)pyrazolo[1,5-*a*]pyrimidine-3-carboxamide (18)** The title compound was prepared as a white solid after trituration with diisopropyl ether in 35% yield from **33** and 3-methyl-1*H*-1,2,4-triazole using the procedure analogous to that described for the synthesis of **14**, except that basic silica gel was employed in a column chromatography purification in place of silica gel. ¹H-NMR (300 MHz, DMSO-*d*₆) δ: 1.02 (3H, brs), 1.36 (3H, s), 2.47 (3H, brs), 4.86 (1H, d, *J*=8.1 Hz), 5.43 (1H, s), 7.21–7.35 (2H, m), 7.47–7.59 (2H, m), 7.63 (1H, d, *J*=7.5 Hz), 8.52 (1H, s), 9.06 (1H, d, *J*=8.1 Hz), 9.46 (1H, d, *J*=7.5 Hz), 9.55 (1H, s). MS (ESI/APCI) *m/z* 476.1 [M+H]⁺. HPLC purity: 100%.

***(S)*-*N*-(2-Hydroxy-2-methyl-1-(4-(trifluoromethoxy)-phenyl)propyl)-6-methyl-5-(4-methyl-1*H*-1,2,3-triazol-1-yl)pyrazolo[1,5-*a*]pyrimidine-3-carboxamide (19)** To a mixture of **52a** (2.81 g, 10.9 mmol) and **28** (3.26 g, 11.4 mmol) in DMF (250 mL) were added HOBt·H₂O (2.06 g, 13.1 mmol), EDCI·HCl (2.55 g, 13.1 mmol) and triethylammonium acetate (TEA) (7.65 mL, 54.4 mmol). The mixture was stirred at r.t. overnight and then quenched with water at r.t. The mixture was extracted with EtOAc, washed with saturated aqueous NaHCO₃, water, and then saturated aqueous NaCl, dried over anhydrous Na₂SO₄, and concentrated *in vacuo*. The residue was purified by column chromatography (silica gel, hexane–ethyl acetate, 100:0 to 3:17) to give **19** (3.86 g, 7.89 mmol, 73%) as a white solid. ¹H-NMR (300 MHz, CDCl₃) δ: 1.17 (3H, s), 1.48 (3H, s), 1.74 (1H, s), 2.50 (3H, d, *J*=0.8 Hz), 2.84 (3H, d, *J*=0.8 Hz), 5.05 (1H, d, *J*=8.3 Hz), 7.17 (2H, d, *J*=7.9 Hz), 7.38–7.48 (2H, m), 8.60 (1H, s), 8.69–8.82 (3H, m). The obtained product (3.86 g, 7.89 mmol) was dissolved in EtOAc (277 mL) at 50–60°C. To this solution was added hexane (150 mL) at the same temperature and a white solid precipitated. After 2 h of stirring at r.t., further hexane (88 mL) was added to the mixture, which was stirred at r.t. for 10 min. The white precipitate was collected by filtration, washed with hexane–ethyl acetate, and dried to give **19** (3.17 g, 6.48 mmol, 82%) as a white solid. ¹H-NMR (300 MHz, CDCl₃) δ: 1.17 (3H, s), 1.48 (3H, s), 1.74 (1H, s), 2.50 (3H, d, *J*=0.8 Hz), 2.84 (3H, d, *J*=0.8 Hz), 5.05 (1H, d, *J*=8.3 Hz), 7.17 (2H, d, *J*=8.3 Hz), 7.39–7.48 (2H, m), 8.60 (1H, s), 8.69–8.83 (3H, m). MS (ESI/APCI) *m/z* 490.2 [M+H]⁺. HPLC purity: 100%. mp 238–239°C. *Anal.* Calcd for C₂₂H₂₂F₃N₇O₃: C, 53.99; H, 4.53; F, 11.64; N, 20.03. Found: C, 53.82; H, 4.42; F, 11.64; N, 19.81.

***(S)*-*N*-(2-Hydroxy-2-methyl-1-(4-(trifluoromethoxy)-phenyl)propyl)-6-methyl-5-(3-methyl-1*H*-1,2,4-triazol-1-yl)pyrazolo[1,5-*a*]pyrimidine-3-carboxamide (20)** To a suspension of **52b** (606 mg, 2.35 mmol) in DMF (12 mL) were added **28** (805 mg, 2.82 mmol), EDCI·HCl (540 mg, 2.82 mmol), HOBt·H₂O (431 mg, 2.82 mmol), and TEA (0.392 mL, 2.82 mmol) at r.t. The mixture was stirred at r.t. for 2 h. The mixture was poured into water and extracted with EtOAc. The organic layer was separated, washed with saturated aqueous NaCl, dried over anhydrous MgSO₄ and concentrated *in vacuo*. The residue was purified by column chromatography (basic silica gel, hexane–ethyl acetate, 4:1 to 1:9) to give **20** (858 mg, 1.75 mmol, 75%) as a white solid after recrystallization from diisopropyl ether/ethyl acetate. ¹H-NMR

(300 MHz, DMSO- d_6) δ : 1.00 (3H, s), 1.31 (3H, s), 2.46 (3H, s), 2.64 (3H, d, $J=0.8$ Hz), 4.87 (1H, d, $J=8.0$ Hz), 5.32 (1H, s), 7.27 (2H, d, $J=8.0$ Hz), 7.51 (2H, d, $J=8.7$ Hz), 8.49 (1H, s), 8.85 (1H, d, $J=8.3$ Hz), 9.46–9.53 (2H, m). MS (ESI/APCI) m/z 490.3 [M+H]⁺. HPLC purity: 100%. mp 212°C. Anal. Calcd for C₂₂H₂₂F₃N₇O₃: C, 53.99; H, 4.53; N, 20.03. Found: C, 54.11; H, 4.50; N, 20.04.

2-Amino-2-(4-(trifluoromethoxy)phenyl)acetic Acid (23)

The solution of potassium cyanide (19.4 g, 299 mmol) in water (170 mL) at 50°C was added dropwise to a solution of 4-trifluoromethoxy benzaldehyde (**21**) (34.1 mL, 239 mmol) and ammonium carbonate (62.0 g, 645 mmol) in EtOH (273 mL) and water (109 mL). The mixture was stirred at 60°C for 3 h. After cooling to r.t., EtOH was removed under reduced pressure. To the mixture was acidified to pH *ca.* 1 with concd HCl at 0°C. The solid was filtered off and washed with water. To a solution of potassium hydroxide (66.2 g, 1000 mmol) in water (250 mL) was added the product at r.t. The mixture was stirred at 90°C overweekend. After cooling to r.t., the mixture was neutralized with concd HCl. The resulting solid was filtered off, washed with water, and dried to give **23** (56.0 g, 238 mmol, 100%) as a pale yellow solid. This was used in the next reaction without further purification. MS (ESI/APCI) m/z 234.0 [M-H]⁻.

(tert-Butoxycarbonyl)amino(4-(trifluoromethoxy)phenyl)acetic Acid (24) To a solution of **23** (56.0 g, 238 mmol) in THF (476 mL) was added Boc₂O (82.9 mL, 357 mmol) and 2 M NaOH aqueous solution (357 mL, 714 mmol) at r.t. The mixture was stirred at r.t. The mixture was poured into water at r.t. and extracted with Et₂O. The aqueous layer was acidified to pH *ca.* 3 with 1 M HCl aqueous solution at 0°C and then extracted with EtOAc. The organic layer was washed with saturated aqueous NaCl, dried over anhydrous MgSO₄ and concentrated *in vacuo* to afford **24** (63.3 g, 189 mmol) as a pale yellow solid. This was subjected to the next reaction without further purification. MS (ESI/APCI) m/z 333.9 [M-H]⁻.

tert-Butyl (2-Hydroxy-2-methyl-1-(4-(trifluoromethoxy)phenyl)propyl)carbamate (25) To a solution of **24** (63.3 g, 189 mmol) in DMF (378 mL) were added MeI (14.2 mL, 227 mmol) and K₂CO₃ (31.3 g, 227 mmol) at r.t. The mixture was stirred at r.t. for 2 h. The mixture was poured into water at r.t. and extracted with EtOAc. The organic layer was separated, washed with saturated aqueous NaCl, dried over anhydrous MgSO₄ and concentrated *in vacuo*. The residue was purified by column chromatography (silica gel, hexane–ethyl acetate, 100:0 to 4:1) to give **25** (38.7 g, 111 mmol, 46% from **21**) as an off-white solid. ¹H-NMR (300 MHz, CDCl₃) δ : 1.26–1.53 (9H, m), 3.73 (3H, s), 5.27–5.41 (1H, m), 5.54–5.75 (1H, m), 7.20 (2H, d, $J=8.3$ Hz), 7.35–7.44 (2H, m). MS (ESI/APCI) m/z 348.1 [M-H]⁻.

tert-Butyl (2-Hydroxy-2-methyl-1-(4-(trifluoromethoxy)phenyl)propyl)carbamate (26) To a solution of **25** (23.5 g, 67.3 mmol) in THF (336 mL) was added dropwise MeMgBr (269 mL, 269 mmol) at 0°C. The mixture was stirred at 0°C under Ar for 1 h. The mixture was quenched with saturated aqueous NH₄Cl at 0°C and extracted with EtOAc. The organic layer was separated, washed with saturated aqueous NaCl, dried over anhydrous MgSO₄ and concentrated *in vacuo*. The residue was purified by column chromatography (silica gel, hexane–ethyl acetate, 19:1 to 2:3) to give **26** (17.9 g,

51.2 mmol, 76%) as a white solid. ¹H-NMR (300 MHz, CDCl₃) δ : 1.05 (3H, s), 1.30–1.47 (12H, m), 4.50 (1H, d, $J=6.4$ Hz), 5.53 (1H, d, $J=8.7$ Hz), 7.18 (2H, d, $J=7.9$ Hz), 7.33 (2H, d, $J=8.7$ Hz). MS (ESI/APCI) m/z 348.0 [M-H]⁻.

tert-Butyl ((1S)-2-Hydroxy-2-methyl-1-(4-(trifluoromethoxy)phenyl)propyl)carbamate (27a) Resolution of the enantiomers of **26** was carried out chromatographically using a Chiralpak AD 20 mm ID×250 mm L column (hexane–ethanol, 950:50) at 80 mL/min. Resolution of **26** (22.3 g, 63.8 mmol) provided **27a** as a white solid (10.2 g, 29.1 mmol, 46%, 91% theoretical) as the first eluting enantiomer. Analytical HPLC analysis carried out on a 4.6 mm ID×250 mm L Chiralpak AD column with the same eluent as above at a flow rate of 1.0 mL/min indicated that **27a** was of >99.9% ee. ¹H-NMR (300 MHz, CDCl₃) δ : 1.05 (3H, s), 1.36 (3H, s), 1.40 (9H, brs), 1.51 (1H, brs), 4.50 (1H, d, $J=7.5$ Hz), 5.53 (1H, d, $J=8.3$ Hz), 7.13–7.23 (2H, m), 7.29–7.39 (2H, m).

(1S)-1-Amino-2-methyl-1-(4-(trifluoromethoxy)phenyl)propan-2-ol Hydrochloride (28) A mixture of **27a** (10.2 g, 29.3 mmol) and 4 M HCl solution in EtOAc (70.0 mL, 280 mmol) was stirred at r.t. for 1.5 h. The mixture was concentrated *in vacuo* and the resulting solid was triturated with hexane–diisopropyl ether, collected by filtration, rinsed with hexane–diisopropyl ether, and dried to afford **28** (7.00 g, 24.5 mmol, 84%) as a pale red solid. ¹H-NMR (300 MHz, DMSO- d_6) δ : 0.98 (3H, s), 1.23 (3H, s), 4.23 (1H, brs), 5.39 (1H, s), 7.37–7.48 (2H, m), 7.63 (2H, d, $J=8.7$ Hz), 8.46 (3H, brs).

Ethyl 5-Hydroxypyrazolo[1,5-*a*]pyrimidine-3-carboxylate (30) To a mixture of ethyl 3-amino-1*H*-pyrazole-4-carboxylate (**29**) (30.0 g, 193 mmol) and ethyl 3-ethoxy-2-propeanoate (*cis*- and *trans*-mixture, 41.9 mL, 290 mmol) in DMF (387 mL) was added cesium carbonate (113 g, 348 mmol). The mixture was stirred at 100°C for 2 h, diluted with water and then acidified to pH *ca.* 5 with AcOH. The resulting solid was filtered by filtration, washed with water and dried to afford **30** (36.4 g, 176 mmol, 91%) as a beige solid. ¹H-NMR (300 MHz, DMSO- d_6) δ : 1.28 (3H, t, $J=7.1$ Hz), 4.28 (2H, q, $J=7.1$ Hz), 6.15 (1H, d, $J=7.9$ Hz), 8.13 (1H, s), 8.57 (1H, d, $J=7.9$ Hz), 11.73 (1H, brs).

5-Hydroxypyrazolo[1,5-*a*]pyrimidine-3-carboxylic Acid (31) To a solution of **30** (20.8 g, 100 mmol) in THF (223 mL) and EtOH (111 mL) was added 2 M NaOH aqueous solution (201 mL, 401 mmol). The mixture was stirred at 50°C overnight. The mixture was evaporated under reduced pressure to remove solvents and then neutralized with 2 M HCl aqueous solution (201 mL, 401 mmol). The resulting solid was collected by filtration, rinsed with water/EtOH and dried to give **31** (17.7 g, 99 mmol, 98%) as a beige solid. ¹H-NMR (300 MHz, DMSO- d_6) δ : 6.14 (1H, d, $J=7.9$ Hz), 8.09 (1H, s), 8.56 (1H, d, $J=7.9$ Hz).

5-Chloropyrazolo[1,5-*a*]pyrimidine-3-carbonyl Chloride (32) To cooled (0°C) POCl₃ (71.0 mL, 762 mmol) were added **31** (5.00 g, 27.9 mmol) and DIEA (16.1 mL, 92.1 mmol). The mixture was stirred at 130°C for 4 h and then concentrated *in vacuo*. The residue was diluted with toluene and water at 0°C, and then extracted with EtOAc. The organic layer was separated, dried over anhydrous Na₂SO₄, filtered through a cake of silica gel pad (eluted with ethyl acetate) and concentrated *in vacuo*. The resulting solid was triturated with heptane, collected by filtration, washed with heptane and dried to give **32**

(4.46 g, 20.7 mmol, 74%) as a beige solid. $^1\text{H-NMR}$ (300 MHz, CDCl_3) δ : 7.16 (1H, d, $J=7.2$ Hz), 8.65 (1H, s), 8.70 (1H, d, $J=7.2$ Hz).

5-Chloro-*N*-((1*S*)-2-hydroxy-2-methyl-1-(4-(trifluoromethoxy)phenyl)propyl)pyrazolo[1,5-*a*]pyrimidine-3-carboxamide (33) To a cooled (0°C) mixture of **32** (1.48 g, 6.85 mmol) and CH_3CN (30 mL) were added **28** (1.96 g, 6.85 mmol) and DIEA (3.58 mL, 20.6 mmol), and the mixture was stirred at 0°C to r.t. for 16 h. The mixture was poured into water and extracted with EtOAc. The organic layer was separated, washed with saturated aqueous NaCl, dried over anhydrous Na_2SO_4 , and concentrated *in vacuo*. The residue was purified by column chromatography (silica gel, hexane–ethyl acetate, 100:0 to 0:100) to give **33** (2.27 g, 5.29 mmol, 77%) as white amorphous solids. $^1\text{H-NMR}$ (300 MHz, CDCl_3) δ : 1.19 (3H, s), 1.40 (3H, s), 1.88 (1H, s), 5.12 (1H, d, $J=8.7$ Hz), 6.99 (1H, d, $J=7.2$ Hz), 7.17–7.23 (2H, m), 7.45–7.53 (2H, m), 8.56 (1H, d, $J=8.7$ Hz), 8.62 (1H, s), 8.67 (1H, d, $J=7.2$ Hz). MS (ESI/APCI) m/z 429.1 $[\text{M}+\text{H}]^+$.

***N*-((1*S*)-2-Hydroxy-2-methyl-1-(4-(trifluoromethoxy)phenyl)propyl)-5-(prop-1-en-2-yl)pyrazolo[1,5-*a*]pyrimidine-3-carboxamide (34)** Into a microwave vial equipped with a magnetic stirrer were added **33** (76.1 mg, 0.177 mmol), 4,4,5,5-tetramethyl-2-(prop-1-en-2-yl)-1,3,2-dioxaborolane (46.6 mg, 0.266 mmol), K_2CO_3 (36.8 mg, 0.266 mmol), toluene (4 mL) and water (0.4 mL), followed by $(\text{Amphos})_2\text{PdCl}_2$ (12.6 mg, 0.0177 mmol). The reaction vial was flushed with nitrogen, sealed and heated by microwave irradiation at 150°C for 25 min. The mixture was purified by column chromatography (basic silica gel, hexane–ethyl acetate, 19:1 to 1:4), followed by a second column purification (silica gel, hexane–ethyl acetate, 19:1 to 1:4) to afford **34** (48.8 mg, 0.112 mmol, 63%) as a yellow amorphous solid. $^1\text{H-NMR}$ (300 MHz, $\text{DMSO-}d_6$) δ : 1.00 (3H, s), 1.27 (3H, s), 2.37 (3H, s), 4.88–4.98 (2H, m), 5.80 (1H, s), 6.36 (1H, s), 7.24–7.34 (2H, m), 7.49–7.58 (2H, m), 7.65 (1H, d, $J=7.5$ Hz), 8.45 (1H, s), 9.02 (1H, d, $J=8.7$ Hz), 9.22 (1H, d, $J=7.5$ Hz). MS (ESI/APCI) m/z 435.2 $[\text{M}+\text{H}]^+$.

5-(3,6-Dihydro-2*H*-pyran-4-yl)-*N*-((1*S*)-2-hydroxy-2-methyl-1-(4-(trifluoromethoxy)phenyl)propyl)pyrazolo[1,5-*a*]pyrimidine-3-carboxamide (35) Into a microwave vial equipped with a magnetic stirrer were added **33** (142 mg, 0.330 mmol), 2-(3,6-dihydro-2*H*-pyran-4-yl)-4,4,5,5-tetramethyl-1,3,2-dioxaborolane (104 mg, 0.495 mmol), K_2CO_3 (68.5 mg, 0.495 mmol), toluene (4 mL) and water (0.4 mL), followed by $(\text{Amphos})_2\text{PdCl}_2$ (23.4 mg, 0.0330 mmol). The reaction vial was flushed with nitrogen, sealed, and heated by microwave irradiation at 150°C for 25 min. The mixture was purified by column chromatography (silica gel, hexane–ethyl acetate, 19:1 to 1:4) to afford **35** (110 mg, 0.230 mmol, 70%) as a yellow solid. $^1\text{H-NMR}$ (300 MHz, $\text{DMSO-}d_6$) δ : 1.00 (3H, s), 1.28 (3H, s), 2.67–2.94 (2H, m), 3.84–3.97 (2H, m), 4.35–4.43 (2H, m), 4.86–5.00 (2H, m), 7.24–7.34 (3H, m), 7.49–7.56 (2H, m), 7.59 (1H, d, $J=7.5$ Hz), 8.42 (1H, s), 9.06 (1H, d, $J=8.7$ Hz), 9.20 (1H, d, $J=7.5$ Hz). MS (ESI/APCI) m/z 477.2 $[\text{M}+\text{H}]^+$.

Ethyl 5-Chloropyrazolo[1,5-*a*]pyrimidine-3-carboxylate (36) POCl_3 (30 mL, 322 mmol) was added to **30** (5.54 g, 26.7 mmol) and the mixture was stirred at 100°C for 16 h. After POCl_3 was removed under reduced pressure, the residue was partitioned between EtOAc and NaHCO_3 aqueous solution. The phases were separated and the aqueous phase was

extracted with EtOAc. The combined organic phases were washed with water and saturated aqueous NaCl, dried over anhydrous Na_2SO_4 and concentrated *in vacuo*. The residue was purified by column chromatography (silica gel, hexane–ethyl acetate, 19:1 to 1:1) to afford **36** (3.69 g, 16.3 mmol, 61%) as a white solid. MS (ESI/APCI) m/z 226.1 $[\text{M}+\text{H}]^+$.

Ethyl 5-(Pyridin-2-yl)pyrazolo[1,5-*a*]pyrimidine-3-carboxylate (38) A mixture of ethyl **36** (300 mg, 1.33 mmol), lithium 4-methyl-1-(pyridin-2-yl)-2,6,7-trioxa-1-borabicyclo[2.2.2]-octan-1-uide (**37**) (566 mg, 2.66 mmol), Ph_3P (139 mg, 0.532 mmol), copper(I) iodide (127 mg, 0.665 mmol) and $\text{Pd}(\text{OAc})_2$ (29.9 mg, 0.133 mmol) in DMF (5 mL) was stirred at 80°C for 2 h under Ar. The mixture was filtered through a cake of basic silica gel pad (eluted with ethyl acetate), followed by a cake of silica gel pad (eluted with ethyl acetate). The appropriate fractions were concentrated *in vacuo*. The resulting solid was triturated with hot ethyl acetate and insoluble materials were filtered off. After concentration of the filtrate, the residue was purified by column chromatography (basic silica gel, hexane–ethyl acetate, 100:0 to 3:7) to give **38** (309 mg, 1.15 mmol, 87%) as a pale yellow solid after trituration with diisopropyl ether. $^1\text{H-NMR}$ (300 MHz, CDCl_3) δ : 1.47 (3H, t, $J=7.1$ Hz), 4.46 (2H, q, $J=7.1$ Hz), 7.40–7.47 (1H, m), 7.86–7.95 (1H, m), 8.25 (1H, d, $J=7.4$ Hz), 8.59 (1H, s), 8.71–8.76 (2H, m), 8.80 (1H, d, $J=7.4$ Hz). MS (ESI/APCI) m/z 269.1 $[\text{M}+\text{H}]^+$.

5-(Pyridin-2-yl)pyrazolo[1,5-*a*]pyrimidine-3-carboxylic Acid (39) A mixture of **38** (117 mg, 0.436 mmol), 4M NaOH aqueous solution (0.545 mL, 2.18 mmol), THF (3.5 mL) and EtOH (3.5 mL) was stirred at 60°C for 2 h. After being cooled to 0°C, the mixture was acidified with 6M HCl aqueous solution (0.363 mL) and concentrated *in vacuo* to give crude **39** (79.0 mg, 0.329 mmol, 75%). This was used in the next reaction without further purification.

tert-Butyl 2-Cyano-3-(dimethylamino)acrylate (42) A mixture of *tert*-butyl 2-cyanoacetate (**40**) (24.3 g, 172 mmol) and *tert*-butoxy bis(dimethylamino)methane (**41**) (35.5 mL, 172 mmol) was stirred at r.t. for 30 min. The mixture was evaporated to give **42** as a pale yellow solid. This was used in the next reaction without further purification. $^1\text{H-NMR}$ (300 MHz, CDCl_3) δ : 1.50 (9H, s), 3.17 (3H, s), 3.36 (3H, s), 7.62 (1H, s).

tert-Butyl 3-Amino-1*H*-pyrazole-4-carboxylate (43) A mixture of **42** (33.8 g, 172 mmol) and hydrazine monohydrate (8.39 mL, 172 mmol) in MeOH (344 mL) was stirred at 70°C overnight. After cooling to r.t., the mixture was poured into water at r.t. and extracted with EtOAc. The organic layer was separated, washed with saturated aqueous NaCl, dried over anhydrous MgSO_4 and concentrated *in vacuo*. The residue was crystallized from diisopropyl ether to give **43** (20.0 g, 109 mmol, 64%) as a pale orange solid. $^1\text{H-NMR}$ (300 MHz, $\text{DMSO-}d_6$) δ : 1.47 (9H, s), 4.86–6.14 (2H, m), 7.07–7.92 (1H, m), 11.44–12.34 (1H, m). MS (ESI/APCI) m/z 184.1 $[\text{M}+\text{H}]^+$.

Methyl 2,3-Dibromo-2-methylpropanoate (45) To a solution of methyl methacrylate (60.1 g, 600 mmol) in EtOAc (353 mL) at 0°C was added a solution of bromine (30.7 mL, 600 mmol) in EtOAc (30 mL). The mixture was stirred at r.t. for 16 h and then saturated aqueous $\text{Na}_2\text{S}_2\text{O}_3$ was added. The mixture was diluted with water and extracted with EtOAc. The combined organic phases were washed with saturated aqueous NaCl, dried over anhydrous Na_2SO_4 and concentrated

in vacuo to afford **45** (152 g, 584 mmol, 97%) as a colorless oil. ¹H-NMR (300 MHz, DMSO-*d*₆) δ: 1.95 (3H, s), 3.76 (3H, s), 4.08–4.14 (1H, m), 4.16–4.22 (1H, m).

Methyl 3,3-Dimethoxy-2-methylpropanoate (46) A suspension of sodium methoxide (28% MeOH solution, 226 g, 1.17 mol) in MeOH (234 mL) was heated to 70°C and then a solution of **45** (152 g, 584 mmol) in MeOH (20 mL) was added rapidly. The mixture was stirred at 70°C for 3 h. After cooling to r.t., the mixture was filtered and washed with MeOH, and then the filtrate was concentrated *in vacuo*. The residue was partitioned between Et₂O and water. The organic layer was washed with water and saturated aqueous NaCl, dried over anhydrous MgSO₄, filtered, and concentrated *in vacuo* to give **46** (54.5 g, 336 mmol, 58%) as a pale yellow oil. This was used in the next reaction without further purification. ¹H-NMR (300 MHz, CDCl₃) δ: 1.17 (3H, d, *J*=7.2 Hz), 2.71–2.85 (1H, m), 3.35 (3H, s), 3.38 (3H, s), 3.70 (3H, s), 4.50 (1H, d, *J*=7.6 Hz).

tert-Butyl 5-Hydroxy-6-methylpyrazolo[1,5-*a*]pyrimidine-3-carboxylate (47) To a mixture of **43** (20.0 g, 109 mmol) and **46** (26.6 g, 164 mmol) in DMF (219 mL) was added cesium carbonate (64.2 g, 197 mmol). The mixture was stirred at 100°C for 16 h, diluted with water and then acidified to pH ca. 4 with AcOH. The resulting solid was filtered by filtration, washed with water and dried to afford **47** (22.6 g, 91.8 mmol, 84%) as a white solid. ¹H-NMR (300 MHz, DMSO-*d*₆) δ: 1.53 (9H, s), 1.96 (3H, d, *J*=1.1 Hz), 7.97 (1H, s), 8.53 (1H, d, *J*=1.1 Hz), 11.22 (1H, brs). MS (ESI/APCI) *m/z* 250.1 [M+H]⁺.

tert-Butyl 5-Azido-6-methylpyrazolo[1,5-*a*]pyrimidine-3-carboxylate (48) To a suspension of **47** (4.99 g, 20.0 mmol) in THF (100 mL) was added 1,8-diazabicyclo[5.4.0]undec-7-ene (DBU) (4.52 mL, 30.0 mmol) and DPPA (5.17 mL, 24.0 mmol) at r.t. The mixture was stirred at 60°C under Ar for 3 h. DBU (1.51 mL, 10.0 mmol) and DPPA (1.72 mL, 8.00 mmol) were added thereto. The mixture was stirred at 60°C under Ar for 2 h. The mixture was poured into water at r.t. and extracted with a 1:1 mixture of hexane and EtOAc. The organic layer was separated, washed with saturated aqueous NaCl, dried over anhydrous MgSO₄, filtered through a short pad of silica gel, eluted with a 1:1 mixture of hexane and EtOAc, and concentrated *in vacuo*. The resulting solid was triturated with hexane to give **48** (4.03 g, 14.7 mmol, 74%) as a pale green solid. ¹H-NMR (300 MHz, DMSO-*d*₆) δ: 1.51–1.65 (9H, m), 2.12–2.55 (3H, m), 8.38–8.49 (1H, m), 8.85–9.11 (1H, m). MS (ESI/APCI) *m/z* 275.1 [M+H]⁺.

tert-Butyl 6-Methyl-5-(4-methyl-1*H*-1,2,3-triazol-1-yl)pyrazolo[1,5-*a*]pyrimidine-3-carboxylate (51a) A mixture of **48** (4.36 g, 15.9 mmol) and **49** (6.07 g, 19.1 mmol) in toluene (79 mL) was stirred at 80°C for 3 h. To the mixture was added MgCl₂ (4.54 g, 47.7 mmol). After 15 min, to the mixture was added MgCl₂ (3.03 g, 31.8 mmol). The mixture was stirred at 60°C under Ar for 2 h. The solid was filtered off, washed with hot toluene. The filtrate was evaporated. The residue was purified by column chromatography (silica gel, hexane–ethyl acetate, 19:1 to 9:11) to give **51a** (4.83 g, 15.4 mmol, 97%) as a white solid. ¹H-NMR (300 MHz, CDCl₃) δ: 1.64 (9H, s), 2.46 (3H, d, *J*=0.8 Hz), 2.78 (3H, d, *J*=1.1 Hz), 8.46–8.50 (2H, m), 8.71–8.73 (1H, m). MS (ESI/APCI) *m/z* 315.2 [M+H]⁺.

6-Methyl-5-(4-methyl-1*H*-1,2,3-triazol-1-yl)pyrazolo[1,5-*a*]pyrimidine-3-carboxylic Acid (52a) To a stirred suspension of **51a** (2.64 g, 8.40 mmol) in CH₃CN (84 mL) was

added methanesulfonic acid (2.78 mL, 42.0 mmol) at 0°C. The mixture was stirred at r.t. overnight. The starting material remained on TLC and further methanesulfonic acid (0.555 mL, 8.40 mmol) was added. The mixture was stirred at r.t. for 1 h and then neutralized with 1 M NaOH aqueous solution at 0°C. The organic solvent was evaporated under reduced pressure and then diluted with water. The resulting solid was collected by filtration, washed with water and then hexane, and dried to give **52a** (1.98 g, 7.67 mmol, 91%) as a white solid. ¹H-NMR (300 MHz, DMSO-*d*₆) δ: 2.40 (3H, s), 2.52 (3H, d, *J*=0.8 Hz), 8.50 (1H, d, *J*=1.1 Hz), 8.62 (1H, s), 9.50 (1H, d, *J*=1.1 Hz), 12.52 (1H, brs). MS (ESI/APCI) *m/z* 259.2 [M+H]⁺.

tert-Butyl 5-Chloro-6-methylpyrazolo[1,5-*a*]pyrimidine-3-carboxylate (50) Carbon tetrachloride (9.73 mL, 100 mmol) was added to a solution of PPh₃ (27.1 g, 100 mmol) in 1,2-dichloroethane (223 mL) at r.t. The mixture was stirred at the same temperature under N₂ for 30 min. To this mixture was added a suspension of **47** (5.0 g, 20.1 mmol) in 1,2-dichloroethane (111 mL) at r.t. and the resulting mixture was stirred under N₂ at 75–85°C for 4.5 h, and then concentrated *in vacuo*. The residue was partitioned between EtOAc and water. The phases were separated and the aqueous phase was extracted with EtOAc. The combined organic phases were washed with saturated aqueous NaCl, dried over anhydrous Na₂SO₄, and concentrated *in vacuo*. The residue was purified by column chromatography (silica gel, hexane–ethyl acetate, 100:0 to 7:3) to give **50** (4.75 g, 17.7 mmol, 88%) as a white solid. ¹H-NMR (300 MHz, CDCl₃) δ: 1.62 (9H, s), 2.42 (3H, d, *J*=0.9 Hz), 8.40 (1H, s), 8.52 (1H, d, *J*=0.9 Hz).

tert-Butyl 6-Methyl-5-(3-methyl-1*H*-1,2,4-triazol-1-yl)pyrazolo[1,5-*a*]pyrimidine-3-carboxylate (51b) To a solution of **50** (1.08 g, 4.03 mmol) in DMF (20 mL) was added 3-methyl-1*H*-1,2,4-triazole (0.469 g, 5.65 mmol) and K₂CO₃ (0.781 g, 5.65 mmol) at r.t. The mixture was stirred at r.t. overnight and warmed to 60°C for 2 h. After cooling to r.t., water was added to the mixture. The solid was collected by filtration, washed with water, and dried to give **51b** (0.870 g, 2.77 mmol, 69%) as a tan solid. ¹H-NMR (300 MHz, DMSO-*d*₆) δ: 1.56 (9H, s), 2.43 (3H, s), 2.54 (3H, d, *J*=1.1 Hz), 8.56 (1H, s), 9.10 (1H, s), 9.43 (1H, d, *J*=1.1 Hz). MS (ESI/APCI) *m/z* 315.2 [M+H]⁺.

6-Methyl-5-(3-methyl-1*H*-1,2,4-triazol-1-yl)pyrazolo[1,5-*a*]pyrimidine-3-carboxylic Acid (52b) To a suspension of **51b** (0.87 g, 2.77 mmol) in CH₃CN (14 mL) was added MsOH (1.26 mL, 19.4 mmol) at 0°C. After being stirred at r.t. for 5 h, the mixture was warmed to 60°C for 30 min. One molar NaOH aqueous solution (19.4 mL, 19.4 mmol) was added thereto at 0°C. CH₃CN was evaporated. The solid was collected by filtration, washed with water, dried to give **52b** (0.606 g, 2.35 mmol, 85%) as a tan solid. ¹H-NMR (300 MHz, DMSO-*d*₆) δ: 2.42 (3H, s), 2.48–2.53 (3H, m), 8.60 (1H, s), 9.09 (1H, s), 9.44 (1H, d, *J*=1.1 Hz), 12.49 (1H, brs). MS (ESI/APCI) *m/z* 259.1 [M+H]⁺.

Enzyme Assay Protocol

Preparation of Human PDE

Human PDE1A, 3A, 4D2, 5A1, 7B, 8A1, 9A2, and 11A4 enzymes were purchased from BPS Bioscience. Human PDE6AB enzyme was purchased from SB Drug Discovery. Human PDE2A3 full-length gene was transduced into Sf9 cells, and the enzyme was purified by His-tag affinity column and gel filtration. Human PDE10A2 was generated from

COS-7 cells that had been transfected with the full-length gene. The enzymes were stored at -70°C until use.

PDE2A3 Enzyme Inhibitory Assay

PDE activity was measured using an SPA (Scintillation Proximity Assay) (GE Healthcare). To evaluate the inhibitory activity of a compound, $10\ \mu\text{L}$ of serially diluted compounds were incubated with $20\ \mu\text{L}$ of PDE enzyme (final concentration $0.023\ \text{nM}$) in assay buffer ($50\ \text{mM}$ *N*-(2-hydroxyethyl)-piperazine-*N'*-2-ethanesulfonic acid (HEPES)–NaOH, $8.3\ \text{mM}$ MgCl_2 , $1.7\ \text{mM}$ ethylene glycol bis(2-aminoethyl ether)-*N,N,N',N'*-tetraacetic acid (EGTA), and 0.1% bovine serum albumin (BSA) (pH 7.4)) for 30 min at r.t. Final concentration of dimethyl sulfoxide (DMSO) in the reaction solution was 1% . Compounds were tested in duplicate in 96-well half-area plates (Corning) or 384-well OptiPlates (PerkinElmer, Inc.). We used an 8 concentration serial dilution dose response ranging from $100\ \mu\text{M}$ to $10\ \text{pM}$ compound concentrations. To start the reaction, $10\ \mu\text{L}$ of substrate [^3H] cGMP (final concentration $77\ \text{nM}$, PerkinElmer, Inc.) were added to a total volume of $40\ \mu\text{L}$. After 60 min at r.t., $20\ \mu\text{L}$ of $20\ \text{mg/mL}$ yttrium silicate SPA beads containing zinc sulfate were added to terminate the PDE reaction. After resting undisturbed for an additional 60 min, the assay plates were counted in a scintillation counter (PerkinElmer, Inc.) to allow calculation of the inhibition rate. Inhibition rate was calculated based on 0% control wells with enzyme and DMSO, and 100% control wells without enzyme. All IC_{50} values were obtained by fitting the results to the following 4 Parameter Logistic Equation:

$$y = A + (B - A) / (1 + (10^{(C-x) \times D}))$$

where A is the minimum y value, B is the maximum y value, C is $\text{Log}(\text{EC}_{50})$ value, and D is the slope factor.

Human PDE Enzyme Assay

PDE activities were measured using an SPA (GE Healthcare). To evaluate the inhibitory activity, $10\ \mu\text{L}$ of serially diluted compounds were incubated with $20\ \mu\text{L}$ of PDE enzymes (except for PDE1A) in assay buffer ($50\ \text{mM}$ HEPES–NaOH, $8.3\ \text{mM}$ MgCl_2 , $1.7\ \text{mM}$ EGTA, and 0.1% BSA (pH 7.4)) for 30 min at r.t. The PDE1A enzyme assay was performed in a different assay buffer ($50\ \text{mM}$ Tris–HCl, $8.3\ \text{mM}$ MgCl_2 , $0.2\ \text{mM}$ CaCl_2 , 0.1% BSA, and $30\ \text{nM}$ Calmodulin (pH 7.5)). The final concentration of DMSO in the assay was 1% . Compounds were tested in duplicate in 96-well half-area plates (Corning). We used an 4 concentration serial dilution dose response ranging from $10\ \mu\text{M}$ to $10\ \text{nM}$ compound concentrations. To start the reaction, $10\ \mu\text{L}$ of substrate (^3H) cGMP (final concentration $77\ \text{nM}$, PerkinElmer, Inc.) for PDE1A, 5A1, 6AB, 9A2, 10A2, and 11A4 or [^3H] cAMP (final concentration $14.7\ \text{nM}$, PerkinElmer, Inc.) for PDE3A, 4D2, 7B, and 8A1) were added for a final assay volume of $40\ \mu\text{L}$. After 60 min incubation at r.t., $20\ \mu\text{L}$ of $20\ \text{mg/mL}$ yttrium silicate SPA beads containing ZnSO_4 were added to terminate the PDE reaction. After resting undisturbed for more than 120 min, the assay plate was counted in a scintillation counter (PerkinElmer, Inc.) to allow calculation of the inhibition rate.

Transcellular Transport Study Using a Transporter-Expression System Human MDR1-expressing LLC-PK1 cells were cultured with minor modifications to the method reported previously.⁵⁷⁾ The transcellular transport study was performed as reported previously.⁵⁸⁾ In brief, the cells were grown for 7 d in HTS Transwell 96-well permeable support

(pore size $0.4\ \mu\text{m}$, $0.143\ \text{cm}^2$ surface area) with polyethylene terephthalate membrane (Corning Life Sciences, Lowell, MA, U.S.A.) at a density of 1.125×10^5 cells/well. The cells were preincubated with M199 at 37°C for 30 min. Subsequently, transcellular transport was initiated by the addition of M199 either to apical compartments ($75\ \mu\text{L}$) or to basolateral compartments ($250\ \mu\text{L}$) containing $10\ \mu\text{M}$ digoxin, $200\ \mu\text{M}$ lucifer yellow (as a marker for the tightness of the monolayer), and $10\ \mu\text{M}$ test compounds. The assay was terminated by the removal of each assay plate after 2 h. Aliquots ($25\ \mu\text{L}$) from the opposite compartments were mixed with CH_3CN containing alprenolol and diclofenac as internal standards, and then centrifuged. The compound concentrations in the supernatant were measured by LC-MS/MS. The apparent permeability (P_{app}) of test compounds in the receiver wells was determined and the efflux ratio (ER) for the MDR1 membrane permeability test was calculated using the following equation:

$$\text{ER} = P_{\text{app, B to A}} / P_{\text{app, A to B}}$$

where $P_{\text{app, A to B}}$ is the apical-to-basal passive permeability-surface area product and $P_{\text{app, B to A}}$ is the basal-to-apical passive permeability-surface area product.

Phototoxicity Test Phototoxicity assay was carried out as described in the OECD guideline No. 432⁴⁶⁾ with some modifications for a high-throughput screening. BALB/c 3T3 cells were cultured at 37°C under 5% CO_2 in Dulbecco's modified Eagle's medium (DMEM) supplemented with 10% fetal bovine serum, $50\ \text{IU/mL}$ penicillin and $50\ \text{mg/mL}$ streptomycin. Cells were seeded at 2.5×10^3 cells/well in 384-well white plates, and cultured in DMEM supplemented with 10% fetal bovine serum, $2\ \text{mM}$ L-glutamine, $1\ \text{mM}$ sodium pyruvate, $50\ \text{IU/mL}$ penicillin, and $50\ \mu\text{g/mL}$ streptomycin for 1 d. Two 384-well plates per test compound ($50\ \mu\text{M}$) in Earle's Balanced Salt Solution (EBSS) supplemented with $1\ \text{mM}$ HEPES were preincubated for 1 h. One of the two plates was irradiated (+UV) for 60 min with $1.4\text{--}1.7\ \text{mW/cm}^2$ ($5\text{--}6\ \text{J/cm}^2$), whereas the other plate was kept in the dark (–UV). In both plates the treatment medium was replaced with the culture medium and after another 24 h of culture, the cell viability was determined by measuring the cellular ATP content. The cellular ATP content was measured using the Celltiter-Glo™ assay kit (Promega) following the manufacture's instruction. ATP content was calculated as follows. ATP content (% of control) = (relative light unit (RLU) of test compound / RLU of 1% DMSO) $\times 100$.

Estimation of $\text{Log}D$ at pH 7.4 $\text{Log}D_{7.4}$, which is the partition coefficient of the compounds between 1-octanol and aqueous buffer at pH 7.4, was measured using a chromatographic procedure based on a published method.⁵⁹⁾ The instruments utilized were a Waters Alliance 2795 HPLC system and a 2996 UV-Vis detector (Milford, MA, U.S.A.).

Thermodynamic Solubility Measurement Using the Shake-Flask Method The measurement of thermodynamic solubility was carried out as previously described.⁵⁹⁾ Briefly, the drug substances were weighed into Thomson filter vials (Chrom Tech, Inc., Minnesota, U.S.A.). JP1 (pH 1.2), JP2 (pH 6.8), and JP2-containing $20\ \text{mM}$ GCDC were added to the vials. The vials were incubated at 37°C for 18 h and the resulting suspensions were filtered by compressing the vials. The drug concentration of the filtrates was determined using a UHPLC system.

Powder X-Ray Diffraction (PXRD) and Crystallinity

Calculation PXRD patterns were collected using a RINT UltimaIV powder X-ray diffractometer (Rigaku Corp., Tokyo, Japan) according to previously described conditions.⁵⁹ The peak intensities of the crystalline (*I_c*) and non-crystalline (*I_a*) fractions were integrated from the baseline collection according to Herman's method.^{60,61} The crystallinity was calculated using the following equation with an autocrystallinity calculation software (Rigaku).^{61,62}

$$\text{Crystallinity} = I_c \times 100 / (I_c + I_a) \times 100$$

Protein Expression and Purification The PDE2A catalytic domain (578–919) was cloned into a pFastBac vector, for expression in Sf9 cells, utilizing an N-terminal 6×poly-histidine tag containing a TEV cleavage site. Large scale production of recombinant protein was carried out in Sf9 cells. The pellet from 10L of baculovirus infected Sf9 cells was resuspended in 600 mL lysis buffer containing 25 mM Tris pH 7.6, 1 M NaCl, 20 mM imidazole, 5% glycerol, and 3 Roche cOmplete Protease Inhibitor tablets. The cell suspension was homogenized with the Polytron PT-3100, centrifuged for 1 h at 13000 rpm (JA-14 rotor), and the clarified supernatant was brought to 800 mL with lysis buffer before batch binding with 10 mL of Probond Ni resin (Invitrogen) for 2 h at 4°C, rolling. The beads were collected by low speed centrifugation (3500 rpm with JS-4.2 rotor), loaded into a gravity column, and washed slowly overnight with 2 L of wash buffer containing 25 mM Tris pH 7.6, 1 M NaCl, 20 mM imidazole, 5% glycerol. The following day the protein was eluted with buffer containing 25 mM Tris pH 7.9, 50 mM NaCl, 250 mM imidazole, 10% glycerol. The 1.5 mL sample eluted from the Nickel capture step was brought to 9 mL with Mono Q buffer A containing 25 mM Tris pH 7.9, and 10% glycerol. After the full sample volume was bound to the Mono Q column, a salt gradient was applied from 0 M NaCl to ca. 800 mM NaCl in 40 mL. Fractions corresponding to the unphosphorylated protein (identified by MS with MW=40178 Da) were pooled for further purification by size-exclusion chromatography on a Superdex 200 column equilibrated in 1×TBS pH 7.4, 0.5 mM DTT, 1 mM EDTA, 10% glycerol. Peak SEC fractions were collected and concentrated to 12 mg/mL for crystallization.

Crystallization and Structure Determination Crystals suitable for data collection were first grown using the vapor diffusion method in hanging drops at r.t. by adding 0.5 μL protein solution with 1 mM IBMX (1-methyl-3-(2-methylpropyl)-2,3,6,7-tetrahydro-1H-purine-2,6-dione) and 0.5 μL reservoir solution (30% PEG 3350, 0.1 M Tris pH 7.5, and 0.2 M MgCl₂). PDE2A IBMX crystals were soaked in a drop containing 5 mM compound **20**, 31% PEG 3350, 0.1 M Tris pH 7.5, and 0.2 M MgCl₂ for 3 d. Crystals were transferred through a fresh cryo-protected soak drop immediately before being harvested and flash frozen in liquid nitrogen. X-Ray diffraction data was collected at ALS beamline 5.0.2 using a Pilatus3 6M (Dectris) detector from a single cryogenically protected crystal (100 K) at a wavelength of 1 Å. The crystals belong to the space group C121 and contain three enzyme molecules per asymmetric unit. X-Ray diffraction data was reduced using the HKL2000⁶³ software package. The structure was determined by molecular replacement with PHASER within the CCP4 program suite and refined with REFMAC.⁶⁴ Several cycles of model building using MIFIT⁶⁵ and refinement using REFMAC were performed for improving the quality of the model. The

coordinates and structure factors have been deposited in the Protein Data Bank with accession code 5VPI.

Animal Experiments The care and use of animals and the experimental protocols were approved by the Experimental Animal Care and Use Committee of Takeda Pharmaceutical Company Limited.

Pharmacokinetic Analysis in Rat or Mouse Cassette Dosing Compound **20** was administered intravenously (0.1 mg/kg) or orally (1 mg/kg) by cassette dosing to nonfasted male CrI:CD(SD)(IGS) rats (8 W, *n*=3) or male ICR mice (8 W, *n*=3). The combination for a cassette dosing was determined to avoid combinations of compounds with the same molecular weight. The solution of compounds in dimethylacetamide containing 50% (v/v) 1,3 butanediol at 0.1 mg/mL/kg was administered intravenously to isoflurane-anesthetized mice *via* femoral vein. The suspension of compounds in 0.5% methyl cellulose with water was used for vehicle (1 mg/kg) and was administered orally by gavage. After administration, blood samples were collected *via* tail vein by syringes with heparin at 5, 10, 15, 30 min, 1, 2, 4, and 8 h (intravenously (*i.v.*)) and 15, 30 min, 1, 2, 4, and 8 h (*per os* (*p.o.*)), and centrifuged to obtain the plasma fraction. The plasma samples were deproteinized by mixing with acetonitrile followed by centrifugation. The compound concentrations in the supernatant were measured by LC-MS/MS with a standard curve. Pharmacokinetic parameters were calculated by the non-compartmental analysis. The area under the concentration–time curve (*AUC*) and the area under the first moment curve (*AUMC*) were calculated using the linear trapezoidal method. The mean residence time (*MRT*) was calculated as *AUMC/AUC*. The total clearance (*CL*_{total}) was calculated as *dose_{i.v.}/AUC_{i.v.}*. The volume of distribution (*V*_{d_{ss}}) was calculated as *CL_{total} × MRT_{i.v.}*. Oral bioavailability (*F*) was calculated as (*AUC_{p.o.}/dose_{p.o.}*) / (*AUC_{i.v.}/dose_{i.v.}*) × 100.

Brain and Plasma Concentration in Rats Compound **20** was administered orally to Long–Evans rats (male, nonfasted, 7-week old) at 10 mg/kg. Blood and whole brain samples were collected 2 h after oral administration. The blood samples were centrifuged to obtain the plasma fraction. The brain samples were homogenized in saline to obtain the brain homogenate. Compound concentrations were measured in aliquots of rat plasma and brain, which were mixed well with acetonitrile containing an internal standard and then centrifuged. The supernatants were diluted with solvents for LC-MS/MS analysis (mobile phase A: 10 mM ammonium formate–formic acid (100:0.2, v/v), mobile phase B: acetonitrile–formic acid (100:0.2, v/v)). The diluted solutions were injected into an LC-MS/MS (API5000, AB Sciex, Foster City, CA, U.S.A.) equipped with a Shimadzu Shim-pack XR-ODS column (2.2 μm packing particle size, 2.0 mm ID×30 mm L) maintained at 50°C. The chromatographic separation was performed using gradient elution at a flow rate of 0.7 mL/min. The LC time program was as follows: Mobile phase B was held at 5% for 0.1 min, and increased linearly to 95% in 0.1 min. After maintaining B at 95% for another 0.8 min, it was decreased to 5% in 0.01 min, followed by re-equilibration for 0.59 min. The total cycle time for one injection was 1.6 min. Compound **20** was detected using multiple reaction monitoring mode and the transition *m/z* 490.01→240.96. Analyst™ software (version 1.4.2) was used for data acquisition and processing.

In Vivo Occupancy Study *In vivo* target occupancy study

of compound **20** was conducted using LC-MS/MS. Compound **20** was suspended in 0.5% (w/v) methylcellulose in distilled water, and PF-05270430⁶⁶) was dissolved in dimethylacetamide and 1,3-butanediol (1:1). Sprague-Dawley (SD) rats were pretreated with vehicle (*p.o.*, $n=6$) or compound **20** (0.3, 1, 3, 10, 30 mg/kg, *p.o.*, $n=4$ in each group) 2 h before sampling. PF-05270430 (0.1 mg/mL/kg) was administered by bolus intravenous injection *via* lateral tail vein 30 min before sampling. Rats were decapitated, and blood and brain samples (striatum as target tissue and cerebellum as reference tissue) were collected. Brain samples were weighed and saline was added (20% (w/v)), followed by homogenization with Lysing Matrix I beads (MP Biomedicals). Homogenized samples were stored at -30°C until quantification of tracer (PF-05270430) using LC-MS/MS. The supernatants were diluted with solvents for LC-MS/MS analysis (mobile phase A: 10 mM ammonium formate–formic acid (100:0.2, v/v), mobile phase B: acetonitrile–formic acid (100:0.2, v/v)). The diluted solutions were injected into an LC-MS/MS (API5000, AB Sciex) equipped with a Shimadzu Shim-pack XR-ODS (2.2 μm packing particle size, 2.0 mm ID \times 30 mm L) maintained at 50°C . The chromatographic separation was performed using gradient elution at a flow rate of 0.7 mL/min. The LC time program was as follows: Mobile phase B was held at 5% for 0.1 min, and increased linearly to 95% in 0.1 min. After maintaining B at 95% for another 0.8 min, it was decreased to 5% in 0.01 min, followed by re-equilibration for 0.59 min. The total cycle time for one injection was 1.6 min. PF-05270430 was detected using multiple reaction monitoring mode and the transition m/z 432 \rightarrow 386. AnalystTM software (version 1.4.2) was used for data acquisition and processing. Specific tracer binding (B_{SP}) in the striatum was represented as the difference between the tracer concentration in striatum and that in cerebellum. PDE2A occupancy was calculated using the following equation: Occupancy (%) = $(B_{\text{SP, base}} - B_{\text{SP, drug}}) / B_{\text{SP, base}} \times 100$, where $B_{\text{SP, base}}$ and $B_{\text{SP, drug}}$ are the concentrations at baseline (vehicle treatment) and at drug treatment, respectively. Curve fitting of the saturation curve was carried out by nonlinear regression using GraphPad Prism 5.02 (GraphPad Software, Inc., San Diego, CA, U.S.A.).

Measurement of Cyclic Nucleotide Contents in Rat Brain Animals

Five-week-old male Long–Evans rats were purchased from Japan SLC, Inc. (Japan). The rats were housed in groups of 3/cage in a light-controlled room (12 h light/dark cycles with lights on at 07:00). Food and water were provided *ad libitum*. After a one week acclimation period, the six-week-old rats were used for experiments.

Measurements

Compound **20** was suspended in 0.5% (w/v) methylcellulose in distilled water, and was administered in a volume of 2 mL/kg body weight for rats. Rats were administered orally with either vehicle or compound **20** (1, 3, 10 mg/kg) after >1 h of habituation. A microwave fixation system (Muromachi Kikai, Tokyo, Japan) was used to sacrifice unanesthetized rats by exposure of the head to the microwave beam at 2 h after administration of **20**. Brain tissues were isolated and then homogenized in 0.5 mol/L HCl, followed by centrifugation. The concentration of cyclic nucleotides in the supernatant was measured using a cyclic AMP EIA kit or cyclic GMP EIA kit (Cayman Chemical, U.S.A.) following the manufacturer's

instructions. Values were expressed as pmol/mg tissue weight.

Step-through Passive Avoidance Task This task was performed as previously described⁶⁷) with some modifications. This experiment was conducted in 7–8-week-old male Long–Evans rats. The apparatus (Brainscience idea, Osaka, Japan) consisted of an illuminated chamber (25 \times 10 \times 25 cm) connected to a dark chamber (30 \times 30 \times 30 cm) by a sliding door (8 \times 8 cm). On the training day, each animal was subjected to a single pre-training trial 4–6 h before the acquisition trial. The rat was placed in the light chamber, and the sliding door was opened 30 s later. As soon as the rat entered the dark chamber with all four paws, the door was closed. The rat was then allowed to remain in the dark chamber for 30 s before being returned to its home cage. In the acquisition trial, the rat was placed in the light chamber, and the sliding door was opened. The time required for the rat to enter the dark chamber was then recorded. As soon as the rat entered the dark chamber, the door was closed, and an electric shock (0.5 mA, 3 s) was delivered from the floor grid. The rat was then returned to its home cage. The retention test was conducted 24 h later. The rat was again placed in the light chamber with the sliding door. After 30 s, the door was opened and the latency for the rat to cross over into the dark compartment was recorded. If the animal did not enter the dark chamber within 300 s, the retention test was terminated, and the animal was given a ceiling score of 300 s. Vehicle or compound **20** (3 mg/kg) was administered *p.o.* 2 h prior, and saline or MK-801 (0.1 mg/kg) was administered *s.c.* 30 min prior to the acquisition trial. The statistical significance of differences between group latency scores was determined by Wilcoxon's test with significance set at $p \leq 0.05$.

Acknowledgments We acknowledge Mr. Kouta Matsu-miya for metabolite identification studies on **6**, Mr. Mitsuyoshi Nishitani for obtaining the single crystal X-ray structure of **S2**, Ms. Miki Hara for chiral separations, Ms. Shoko Takeuchi for thermodynamic solubility and crystallinity measurements on **19** and **20**, Dr. Gyorgy Snell and Mr. Scott Lane (Takeda California, Inc.) for crystallographic data collection and processing of **20**, and Dr. Toshihiro Imaeda for supplying large amounts of key intermediate **28**.

Conflict of Interest The authors declare no conflict of interest.

Supplementary Materials The online version of this article contains supplementary materials. Synthesis of (+)-di-(*p*-toluoyl)-D-tartaric acid salt (**S2**) of free base of **28** suitable for X-ray crystallography. Synthesis of pyrazolo[1,5-*a*]pyrimidine derivatives **5** and **6**. Full details of the X-ray structure analysis of **S2**. Molecular formula strings.

References

- 1) van Os J., Kapur S., *Lancet*, **374**, 635–645 (2009).
- 2) Tandon R., Keshavan M. S., Nasrallah H. A., *Schizophr. Res.*, **100**, 4–19 (2008).
- 3) Tandon R., Keshavan M. S., Nasrallah H. A., *Schizophr. Res.*, **102**, 1–18 (2008).
- 4) McGrath J., Saha S., Chant D., Welham J., *Epidemiol. Rev.*, **30**, 67–76 (2008).
- 5) Miyamoto S., Duncan G. E., Marx C. E., Lieberman J. A., *Mol.*

- Psychiatry*, **10**, 79–104 (2005).
- 6) Murphy B. P., Chung Y.-C., Park T.-W., McGorry P. D., *Schizophr. Res.*, **88**, 5–25 (2006).
 - 7) Lieberman J. A., Stroup T. S., McEvoy J. P., Swartz M. S., Rosenheck R. A., Perkins D. O., Keefe R. S., Davis S. M., Davis C. E., Lebowitz B. D., Severe J., Hsiao J. K., *N. Engl. J. Med.*, **353**, 1209–1223 (2005).
 - 8) Gothelf D., Apter A., Reidman J., Brand-Gothelf A., Bloch Y., Gal G., Kikinzon L., Tyano S., Weizman R., Ratzoni G., *J. Neural Transm.*, **110**, 545–560 (2003).
 - 9) Ayano G., *J. Schizophr. Res.*, **3**, 1027.1–1027.5 (2016).
 - 10) Niewoehner U., Schauss D., Hendrix M., Koenig G., Boess F. G., van der Staay F. J., Schreiber R., Schlemmer K. H., Grosser R., WO 2002050078, June 27, 2002.
 - 11) Boess F. G., Hendrix M., van der Staay F.-J., Erb C., Schreiber R., van Staveren W., de Vente J., Prickaerts J., Blokland A., Koenig G., *Neuropharmacology*, **47**, 1081–1092 (2004).
 - 12) Rutten K., Van Donkelaar E. L., Ferrington L., Blokland A., Bollen E., Steinbusch H. W. M., Kelly P. A. T., Prickaerts J. H. H. J., *Neuropsychopharmacology*, **34**, 1914–1925 (2009).
 - 13) Bolger G. B., Rodgers L., Riggs M., *Gene*, **149**, 237–244 (1994).
 - 14) Van Staveren W. C., Steinbusch H. W., Markerink-Van Ittersum M., Repaske D. R., Goy M. F., Kotera J., Omori K., Beavo J. A., De Vente J., *J. Comp. Neurol.*, **467**, 566–580 (2003).
 - 15) Reyes-Irisarri E., Markerink-Van Ittersum M., Mengod G., de Vente J., *Eur. J. Neurosci.*, **25**, 3332–3338 (2007).
 - 16) Stephenson D. T., Coskran T. M., Wilhelms M. B., Adamowicz W. O., O'Donnell M. M., Muravnick K. B., Menniti F. S., Kleiman R. J., Morton D., *J. Histochem. Cytochem.*, **57**, 933–949 (2009).
 - 17) Lakics V., Karran E. H., Boess F. G., *Neuropharmacology*, **59**, 367–374 (2010).
 - 18) Stephenson D. T., Coskran T. M., Kelly M. P., Kleiman R. J., Morton D., O'Neill S. M., Schmidt C. J., Weinberg R. J., Menniti F. S., *Neuroscience*, **226**, 145–155 (2012).
 - 19) Bender A. T., Beavo J. A., *Pharmacol. Rev.*, **58**, 488–520 (2006).
 - 20) Frey U., Huang Y. Y., Kandel E. R., *Science*, **260**, 1661–1664 (1993).
 - 21) Son H., Lu Y. F., Zhuo M., Arancio O., Kandel E. R., Hawkins R. D., *Learn. Mem.*, **5**, 231–245 (1998).
 - 22) Lu Y., Kandel E. R., Hawkins R. D., *J. Neurosci.*, **19**, 10250–10261 (1999).
 - 23) Prickaerts J., de Vente J., Honig W., Steinbusch H. W. M., Blokland A., *Eur. J. Pharmacol.*, **436**, 83–87 (2002).
 - 24) Sanderson T. M., Sher E., *Neuropharmacology*, **74**, 86–95 (2013).
 - 25) Abaarghaz M., Biondi S., Duranton J., Limanton E., Mondadori C., Wagner P., WO 2005063723, July 14, 2005.
 - 26) Schmidt B., Weinbrenner S., Flockerzi D., Kuelzer R., Tenor H., Kley H.-P., WO 2006024640, March 9, 2006.
 - 27) Schmidt B., Weinbrenner S., Flockerzi D., Külzer R., Tenor H., Kley H.-P., WO 2006072612, July 13, 2006.
 - 28) Schmidt B., Weinbrenner S., Flockerzi D., Külzer R., Tenor H., Kley H.-P., WO 2006072615, July 13, 2006.
 - 29) Buijnsters P., De Angelis M., Langlois X., Rombouts F. J. R., Sanderson W., Tresadern G., Ritchie A., Trabanco A. A., VanHoof G., Van Roosbroeck Y., Andrés J.-I., *ACS Med. Chem. Lett.*, **5**, 1049–1053 (2014).
 - 30) Rombouts F. J. R., Tresadern G., Buijnsters P., Langlois X., Tovar F., Steinbrecher T. B., Vanhoof G., Somers M., Andrés J.-I., Trabanco A. A., *ACS Med. Chem. Lett.*, **6**, 282–286 (2015).
 - 31) Redrobe J. P., Jørgensen M., Christoffersen C. T., Montezinho L. P., Bastlund J. F., Carnerup M., Bundgaard C., Lerdrup L., Plath N., *Psychopharmacology* (Berl.), **231**, 3151–3167 (2014).
 - 32) Helal C. J., Identification of a Brain Penetrant, Highly Selective Phosphodiesterase 2A Inhibitor for the Treatment of Cognitive Impairment Associated with Schizophrenia (CIAS). 244th National Meeting & Exposition, Philadelphia, PA, United States, August 19–23, 2012.
 - 33) Chappie T. A., Humphrey J. M., Verhoest P. R., Yang E., Helal C. J., WO 2012114222, August 30, 2012.
 - 34) Helal C. J., Chappie T. A., Humphrey J. M., WO 2012168817, December 13, 2012.
 - 35) Mikami S., Nakamura S., Ashizawa T., Sasaki S., Taniguchi T., Nomura I., Kawasaki M., WO 2013161913, October 31, 2013.
 - 36) Nakamura S., Mikami S., Kawasaki M., Nomura I., Ashizawa T., Taniguchi T., WO 2014010732, January 16, 2014.
 - 37) Kawasaki M., Mikami S., Nakamura S., Negoro N., Ikeda S., Nomura I., Ashizawa T., Imaeda T., Seto M., Sasaki S., Marui S., Taniguchi T., WO 2015012328, January 29, 2015.
 - 38) Seto M., Banno Y., Imaeda T., Kajita Y., Ashizawa T., Kawasaki M., Nakamura S., Mikami S., Nomura I., Taniguchi T., Marui S., WO 2015060368, April 30, 2015.
 - 39) Shen D.-M., Egbertson M., Berger R., Qian X., Qian Y., Harper B., Yang M., Zack Z. Q., Rada V. L., Wang D., Cernak T. A., Sinz C. J., Wang M., Wilson J. E., Xu S., WO 2015096651, July 2, 2015.
 - 40) Trabanco A. A., Buijnsters P., Rombouts F. J. R., *Expert Opin. Ther. Pat.*, **26**, 933–946 (2016).
 - 41) Gomez L., Massari M. E., Vickers T., Freestone G., Vernier W., Ly K., Xu R., McCarrick M., Marrone T., Metz M., Yan Y. G., Yoder Z. W., Lemus R., Broadbent N. J., Barido R., Warren N., Schmelzer K., Neul D., Lee D., Andersen C. B., Sebring K., Aertgeerts K., Zhou X., Tabatabaei A., Peters M., Breitenbucher J. G., *J. Med. Chem.*, **60**, 2037–2051 (2017).
 - 42) Mikami S., Sasaki S., Asano Y., Ujikawa O., Fukumoto S., Nakashima K., Oki H., Kamiguchi N., Imada H., Iwashita H., Taniguchi T., *J. Med. Chem.*, **60**, 7658–7676 (2017).
 - 43) Mikami S., Nakamura S., Ashizawa T., Nomura I., Kawasaki M., Sasaki S., Oki H., Kokubo H., Hoffman I. D., Zou H., Uchiyama N., Nakashima K., Kamiguchi N., Imada H., Suzuki N., Iwashita H., Taniguchi T., *J. Med. Chem.*, **60**, 7677–7702 (2017).
 - 44) Hitchcock S. A., Pennington L. D., *J. Med. Chem.*, **49**, 7559–7583 (2006).
 - 45) Hitchcock S. A., *J. Med. Chem.*, **55**, 4877–4895 (2012).
 - 46) OECD, “OECD Guidelines for the Testing of Chemicals, Section 4: Health Effects (Test No. 432: *in vitro* 3T3 NRU Phototoxicity Test). 2004”: http://www.oecd-ilibrary.org/environment/test-no-432-in-vitro-3t3-nru-phototoxicity-test_9789264071162-en?jsessionid=3qtfu6logglhf.x-oecd-live-02, accessed August 9, 2017.
 - 47) Stein K. R., Scheinfeld N. S., *Expert Opin. Drug Saf.*, **6**, 431–443 (2007).
 - 48) Peukert S., Nunez J., He F., Dai M., Yusuff N., DiPesa A., Miller-Moslin K., Karki R., Lagu B., Harwell C., Zhang Y., Bauer D., Kelleher J. F., Egan W., *Med. Chem. Commun.*, **2**, 973–976 (2011).
 - 49) Wager T. T., Hou X., Verhoest P. R., Villalobos A., *ACS Chem. Neurosci.*, **1**, 435–449 (2010).
 - 50) Podzuweit T., Nennstiel P., Müller A., *Cell. Signal.*, **7**, 733–738 (1995).
 - 51) Neill J. C., Barnes S., Cook S., Grayson B., Idris N. F., McLean S. L., Snigdha S., Rajagopal L., Harte M. K., *Pharmacol. Ther.*, **128**, 419–432 (2010).
 - 52) van der Staay F. J., Rutten K., Erb C., Blokland A., *Behav. Brain Res.*, **220**, 215–229 (2011).
 - 53) Ware E., *Chem. Rev.*, **46**, 403–470 (1950).
 - 54) Yamamoto Y., Takizawa M., Yu X.-Q., Miyaura N., *Heterocycles*, **80**, 359–368 (2010).
 - 55) Harvey G. R., *J. Org. Chem.*, **31**, 1587–1590 (1966).
 - 56) L'abbé G., *Angew. Chem. Int. Ed. Engl.*, **14**, 775–782 (1975).
 - 57) Sugimoto H., Hirabayashi H., Kimura Y., Furuta A., Amano N., Moriwaki T., *Drug Metab. Dispos.*, **39**, 8–14 (2011).
 - 58) Takeuchi T., Yoshitomi S., Higuchi T., Ikemoto K., Niwa S., Ebihara T., Katoh M., Yokoi T., Asahi S., *Pharm. Res.*, **23**, 1460–1472 (2006).
 - 59) Yamamoto K., Ikeda Y., *J. Drug Deliv. Sci. Tec.*, **33**, 13–18 (2016).
 - 60) Hermans P. H., Weidinger A., *J. Appl. Phys.*, **19**, 491–506 (1948).

- 61) Ikeda Y., Ban J., Ishikawa T., Hashiguchi S., Urayama S., Horibe H., *Chem. Pharm. Bull.*, **56**, 1406–1411 (2008).
- 62) Yamamura S., Momose Y., *Int. J. Pharm.*, **212**, 203–212 (2001).
- 63) Otwinowski Z., Minor W., *Methods Enzymol.*, **276**, 307–326 (1997).
- 64) Collaborative Computational Project, *Acta Crystallogr. D Biol. Crystallogr.*, **50**, 760–763 (1994).
- 65) Smith B., Badger J., “MIFit, 2010. 10”; <<https://github.com/mifit/mifit>>, June 12, 2010.
- 66) Zhang L., Villalobos A., Beck E. M., Bocan T., Chappie T. A., Chen L., Grimwood S., Heck S. D., Helal C. J., Hou X., Humphrey J. M., Lu J., Skaddan M. B., McCarthy T. J., Verhoest P. R., Wager T. T., Zasadny K., *J. Med. Chem.*, **56**, 4568–4579 (2013).
- 67) Miyamoto M., Takahashi H., Kato K., Hirai K., Ishihara Y., Goto G., *J. Pharmacol. Exp. Ther.*, **277**, 1292–1304 (1996).